Titre: Title:	Effect of an electromagnetic field on natural convection in an inclined porous layer
Auteur: Author:	Fanming Meng
Date:	1994
Type:	Mémoire ou thèse / Dissertation or Thesis
Référence: Citation:	Meng, F. (1994). Effect of an electromagnetic field on natural convection in an inclined porous layer [Master's thesis, École Polytechnique de Montréal]. PolyPublie. https://publications.polymtl.ca/33015/

URL de PolyPublie: PolyPublie URL:	https://publications.polymtl.ca/33015/
Directeurs de recherche: Advisors:	Ertugrul Bilgen, & Patrick Vasseur
Programme: Program:	Unspecified

UNIVERSITÉ DE MONTRÉAL

EFFECT OF AN ELECTROMAGNETIC FIELD ON NATURAL CONVECTION IN AN INCLINED POROUS LAYER

par

Fanming MENG
DÉPARTEMENT DE GÉNIE MÉCANIQUE
ÉCOLE POLYTECHNIQUE

MÈMOIRE PRÉSENTÉ EN VUE DE L'OBTENTION
DU GRADE DE MAÎTRE ÈS SCIENCES APPLIQUÉES (M.Sc.A.)
(GÉNIE MÉCANIQUE)

Juin 1994

ISBN 0-315-97121-5

UNIVERSITÉ DE MONTRÉAL

ÉCOLE POLYTECHNIQUE

Ce mèmoire intitulé:

EFFECT OF AN ELECTROMAGNETIC FIELD ON NATURAL CONVECTION IN AN INCLINED POROUS LAYER

Présenté par: Fanming MENG

en vue de l'obtention du grade de: Maître ès Sciences Appliquées (M.Sc.A.)

a été dûment accepté par le jury d'examen constitué de:

M. ROBILLARD, Luc, Ph.D., Président

M. BILGEN, Ertugrul, Ph.D., directeur de recherche

M. VASSEUR, Patrick, Ph.D., codirecteur

M. ALCHAAR,Samir, Ph.D., membre

SOMMAIRE

Dans cette étude on considere l'effet d'un champ magnétique sur la convection naturelle au sein d'une cavité rectangulaire inclinée contenant un milieu poreux saturé par un fluide électriquement conducteur. Les côtés de la cavité sont maintenus à température constante alors que les bouts sont isolés thermiquement. Un champ magnetique uniforme est appliqué perpendiculairement aux parois chauffées. Le milieu poreux est isotropique et peut être modelisé selon la loi de Darcy. Les equations adimensionnelles de base sont derivées et il est montré que les parametres de base du probléme sont R, le nombre de Rayleigh, Ha le nombre de Hartmann magnetique, A le rapport de forme de la cavité et θ, l'inclinaison de la cavité. Une solution analytique approximée est développée pour le regime de couche limite dans une cavité verticale. Une analyse de stabilité lineaire est presentée afin de déterminer l'effet du champ magnétique sur le nomrbre de Rayleigh critique marquant le début de la convection dans une couche horizontale chauffée pour le bas. Une étude numérique du problème est conduite afin de vérifier et d'étendre les resultats des solutions analytiques. Il est démontré que l'application d'un champ magnetique modifiait considérablement les champs de température et de vitesse. Les relations entre le taux de transfert thermique global, décrit par le nombre de Nusselt moyen et les paramétres de base, sont presentées. Il est observé que le nombre de Nusselt moyen decroit avec un accroisement du nombre de Hartmann. On démontre qu'un champ magnétique peut etre utilisé pour controler la convection dans une cavité.

ABSTRACT

An investigation is conducted to study the effect of an electromagnetic field on free convection of an inclined rectangular porous cavity saturated with an electrically conducting fluid. The enclosure has the long side walls heated isothermally while the short ends are thermally insulated. A uniform magnetic field is applied normal to the heated walls. The porous medium, modeled according to the Darcy's law, is assumed to be isotropic. The dimensionless governing equations are derived in terms of the characteristic dimensionless parameters, namely, the Rayleigh number R, the magnetic Hartmann number Ha, the cavity aspect ratio A and the inclination angle θ. An approximate analytical solution is presented for the boundary layer flow regime within a vertical cavity. A linear stability analysis is made to determine the effect of the magnetic field on the onset of convection in a horizontal layer heated from below. A numerical study is performed to assess and extend the results of the analytical solutions. It is found that with application of an external magnetic field, the temperature and velocity fields are significantly modified. The relationships between the overall heat transfer rate, described by the average Nusselt number and the other governing parameters, are presented. It is observed that the average Nusselt number decreases with increasing Hartmann number; and, the effect of the orientation angle is affected by the imposition of a magnetic field; hence, a magnetic field can be used as an effective mechanism to control the convection in an enclosure.

RESUMÉ

La convection naturelle dans une cavité poreuse chauffée par les côtés a fait l'objet de nombreuses études dans le passé à cause des diverses applications potentielles dans le domaine du génie [1-10]. Tous ces travaux ont été discutés récemment dans un livre par Nield et Bejan [11].

La plupart des investigations disponibles sur ce sujet portent sur le cas d'un milieu poreux saturé par un fluide électriquement non conducteur, ce qui est le cas dans la plupart des situations pratiques. Récemment, le problème de la convection hydromagnétique a été considéré par un certain nombre d'auteurs. Lorsqu'un fluide électriquement conducteur est sujet à un champ magnétique, l'écoulement de ce dernier est retardé par l'interaction entre le courant électrique et le mouvement. Malgré les nombreuses applications possibles, très peu d'études ont considéré la convection naturelle dans un milieu poreux en présence d'un champ magnétique. Ce genre de situation se rencontre par exemple dans les régions géothermales où la croûte terrestre se comporte comme un milieu poreux. En métallurgie, la solidification de la structure peut être considérablement améliorée par un malaxage électromagnétique du métal liquide. Lors de la solidification, les dendrites à l'interface du front de solidification peuvent être considérées comme une région poreuse.

L'interaction d'un champ magnétique externe avec des courants convectifs dans un milieu poreux a été considérée en premier par Raptis et al. [12,13].

Ils ont étudié l'influence d'un champ magnétique horizontal constant sur la convection naturelle dans un milieu poreux bordé par deux plaques verticales infinies. Le cas d'un milieu poreux bordé par une seule plaque a également été considéré par ces auteurs. Singh et Dikshit [14] ont étudié la convection dans le cas de l'écoulement de Couette d'un liquide électriquement conducteur dans un milieu poreux. Des solutions exactes pour les champs d'écoulements ont été obtenues en terme des paramètres de base du problème. Kumar Jha et Prasad [15] ont considéré le mouvement impulsif d'une plaque verticale bordant un milieu poreux. L'effet des différents paramètres sur l'écoulement du fluide était discuté. Une analyse de l'influence du courant de Hall sur la convection naturelle au sein d'un milieu poreux bordé par une plaque verticale a été effectuée par Takhar et Ram [16]. Un champ magnétique intense était imposé selon un angle α avec la direction verticale. L'influence des courants de Hall sur l'écoulement était considéré pour différentes valeurs de α. Récemment, Ni et al. [17] ont analysé l'effet d'un champ magnétique sur la convection naturelle au sein d'une cavité verticale. Des résultats numériques, en terme de la vitesse et du nombre de Nusselt, ont été présentés afin de mieux comprendre l'influence du phénomène électromagnétique sur l'écoulement d'un fluide dans un milieu poreux. Il a été démontré par ces auteurs que pour des grandes valeurs de Ha, l'effet du champ magnétique était de retarder l'écoulement dans le milieu poreux d'une manière similaire au cas d'une matrice poreuse beaucoup moins perméable.

Dans la présente étude, on examine l'effet d'un champ magnétique sur la convection naturelle dans une cavité inclinée contenant un milieu poreux saturé par un fluide électriquement conducteur. Les côtés de la cavité sont

maintenus à température constante alors que les bouts sont isolés thermiquement. Un champ magnétique uniforme est appliqué perpendiculairement aux parois chauffées. Le milieu poreux est isotropique et peut être modélisé selon la loi de Darcy. Les équations adimensionnelles sont dérivées et il est montré que les paramètres de base du problème sont R, le nombre de Rayleigh, Ha le nombre de Hartmann magnétique, A le rapport de forme de la cavité et θ, l'inclinaison de la cavité.

Une solution analytique approximée est développée pour le régime de couche limite dans une cavité verticale. Une analyse de stabilité linéaire est présentée afin de déterminer l'effet de champ magnétique sur le nombre de Rayleigh critique marquant le début de la convection dans une couche horizontale chauffée pour le bas.

Dans le cas général d'une cavité inclinée, une étude numérique de ce problème a été conduite. La méthode utilisée est basée sur la formulation en volume de contrôle proposée par Patankar [19]. Dans cette technique, on intègre les équations de base sur une petite région appelée volume de contrôle. Chaque volume est associé avec un point discret sur lequel des variables telles que la fonction de courant, la vitesse et la température peuvent être calculées. Un schéma de type loi en puissance a été adopté pour la formulation des termes de convection-diffusion. Les équations discrétisées résultantes ont été résolues itérativement en appliquant l'algorithme de Thomas. Dans la procédure numérique, on détermine tout d'abord le champ de température à partir de l'équation d'énergie. Ensuite, la fonction de courant est obtenue en résolvant l'équation de quantité de mouvement en utilisant le champ de température.

Finalement, le champ de vitesse est déterminé à l'aide de la fonction de courant. A partir de la solution numérique, il est démontré que l'application d'un champ magnétique modifiait considérablement les champs de température et de vitesse. Les relations entre le taux de transfert thermique global, décrites par le nombre de Nusselt moyen et les paramètres de base, sont présentées. Il est observé que le nombre de Nusselt moyen décroît avec un accroissement du nombre de Hartmann. On démontre qu'un champ magnétique peut être utilisé pour contrôler la convection dans une cavité.

En résumé, l'effet d'un champ magnétique transversal sur la convection naturelle dans une cavité poreuse inclinée, saturée par un fluide électriquement conducteur, a été étudié analytiquement et numériquement. Les principales conclusions de cette étude sont:

1° Dans le cas d'une cavité verticale chauffée par le côté $(\theta = 90°)$, il a été montré qu'une simple analyse dimensionnelle pouvait prédire correctement le comportement asymptotique du champ de vitesse dans la limite $\underline{R} \to \infty$. On a également obtenu, pour le régime de la couche limite, la dépendance du nombre de Nusselt avec R, A et Ha explicitement en utilisant la méthode intégrale proposée par Simpkins et Blythe [4]. L'expression résultante, $Nu = 0.51\left[R/A(1 + Ha^2)\right]^{1/2}$ a été validée avec des résultats numériques obtenus pour des cavités ayant des rapports de forme $\underline{A} = 4$ et 8.

2° L'effet d'un champ magnétique sur la convection de Bénard, dans

une couche poreuse chauffée par dessous, $\theta = 180°$, a été considéré. Le nombre de Rayleigh critique pour l'apparition de la convection a été prédit, en utilisant la théorie linéaire de la stabilité. Il a été trouvé que le nombre de Rayleigh critique est donné par

$$R_{cr} = \left(1 + \sqrt{Ha^2 + 1}\right)^2 \pi^2 \quad ; \quad \left(\alpha = \pi (Ha^2 + 1)^{1/4}\right)$$

de façon à ce que lorsque Ha = 0, i.e. en l'absence d'un champ magnétique, les formules ci-dessus se réduisent à

$$R_{cr} = 4\pi^2 \quad , \quad \alpha = \pi$$

qui sont les résultats classiques obtenus dans le passé par Lapwood [23]. L'effet d'un champ magnétique est donc de stabiliser la couche poreuse et un nombre de Rayleigh critique supérieur est nécessaire pour engendrer les mouvements de convection.

La convection supercritique au sein d'une cavité chauffée par le bas a été étudiée numériquement. Typiquement, on a considéré le cas A = 6, R = 500 et différentes valeurs de Ha. En l'absence d'un champ magnétique, i.e. quand Ha = 0, les résultats numériques montrent que six cellules ayant approximativement la même dimension occupent la couche poreuse. En augmentant Ha

de 0 à 4, il a été trouvé que les six cellules précédentes étaient remplacées par huit cellules. Cette tendance est en accord avec les résultats de la théorie de la stabilité selon laquelle l'effet du champ magnétique est de décroître la longueur d'onde des cellules de convection $(\alpha = \pi\,(Ha^2 + 1)^{1/4})$. On a également remarqué que l'intensité de la convection était considérablement modifiée par la force de traînée induite par le champ magnétique. En augmentant Ha de 4 à 5, il a été trouvé que dix cellules occupent alors la couche poreuse. Pour cette situation, la convection est très faible et le transfert de chaleur est presque entièrement fait par diffusion.

3° L'effet d'un champ magnétique sur le transfert de chaleur au sein d'une cavité inclinée a été également étudié. Ce problème, en l'absence d'un champ magnétique, a été considéré récemment par Caltagirone et Bories [24] et Moya et al. [25]. Il a été montré par ces auteurs que, pour des angles proches de zéro, le mode préféré de circulation est multicellulaire alors que pour des angles d'inclinaison plus grands, le mode préféré est unicellulaire. L'angle de transition entre les écoulements unicellulaires et multicellulaires dépend du rapport de forme de la cavité et du nombre de Rayleigh. Ce phénomène a également été observé dans la présente étude pour le cas Ra = 500 et A = 4. Dans le cas d'une cavité horizontale $(\theta = 180°)$, les résultats numériques indiquent la présence de quatre cellules de convection. En décroissant l'angle d'inclinaison jusqu'à 175°, le nombre des

cellules de convection passe alors à cinq cellules. Ce dernier type d'écoulement peut être maintenu jusqu'à $\theta \simeq 140°$. Pour des plus petits angles d'inclinaison l'écoulement devient unicellulaire.

Dans la région de transition entre les écoulements multicellulaires et unicellulaires, des effets d'hystérésis ont été observés dans la présente étude. Ainsi, lorsque l'angle d'inclinaison est augmenté de $\theta = 140°$ vers $\theta = 180°$, l'écoulement pour un θ donné ne correspondait pas exactement aux résultats décrits précédemment. Par exemple, l'écoulement unicellulaire observé pour $\theta = 140°$ peut être maintenu jusqu'à $\theta = 170°$. Pour $\theta = 171°$, un écoulement unicellulaire englobant deux cellules secondaires est observé. En augmentant encore l'angle d'inclinaison, les résultats numériques indiquent la présence de trois cellules de convection dans la cavité, ce type d'écoulement se conservant jusqu'à $\theta = 180°$. Ce genre de phénomène ne semble pas avoir été observé dans le passé. Dans le cas où un champ magnétique est présent, ce dernier a un grand effet sur l'angle de transition entre les écoulements unicellulaires et multicellulaires. Par exemple, pour une cavité avec $\underline{A} = 4$ et $\underline{R} = 500$, l'angle de transition est $\theta = 171°$ quand $\underline{Ha} = 0$ mais il est $\theta = 131°$ quand $\underline{Ha} = 3$.

ACKNOWLEDGEMENTS

I would like to express my greatest appreciation to Professor E. Bilgen my advisor and Professor P. Vasseur, my co-advisor, for their encouragement and careful guidance during my research work and feel very pleased to have the opportunity to work under their supervision and counselling in all phases of my graduate studies at École Polytechnique, University of Montreal. They have given me invaluable help in many ways.

Grateful acknowledgements are also expressed to Dr. Bian Wei for his many helpful suggestions and discussions during my graduate study.

Many professors, fellow graduate students, colleagues and friends in the Mechanical Engineering Department of École Polytechnique,University of Montreal have provided a lot of suggestions and personal help. My sincere thanks go to all, and I would like to mention specifically the help and advice that I received from professor Luc Robillard.

Also, acknowledgement is due to the National Sciences and Engineering Research Council of Canada for the financial support for this project as well as Thermo Fluid Group at École Polytechnique that provides a dynamic and exciting atmosphere together with good computer facilities.

TABLE OF CONTENTS

LIST OF FIGURES

LIST OF TABLES

LIST OF SYMBOLS

A	aspect ratio, H/L
$\vec{B}'$	applied magnetic field
g	acceleration due to gravity
H	height of the cavity
Ha	Hartmann number, $B'(K\sigma/\mu)^{1/2}$
$\vec{J}'$	electric current
k	thermal conductivity of fluid-saturated porous medium
K	permeability of fluid-saturated porous medium
l	characteristic length, Eq. (??)
L	thickness of the cavity
Nu	Nusselt number, Eq. (??)
p'	pressure
R	Darcy-Rayleigh number, $Kg\beta L\Delta T'/\alpha_f\nu$
T	dimensionless temperature, $(T' - T'_C)/\Delta T'$
$\Delta T'$	characteristic temperature, $(T'_H - T'_C)$
V'	intrinsic velocity field
u, v	dimensionless velocities in x and y directions,$(u', v')L/\alpha_f$
x, y	dimensionless cartesian coordinates, $(x', y')/L$

Greek Symbols

α	wave length

α_f	effective thermal diffusivity of the porous medium
β	coefficient of thermal expansion of the fluid
θ	inclination angle
μ	dynamic viscosity of fluid
ν	kinematic viscosity of fluid
ρ	fluid density
σ	electrical conductivity
ϕ	electric potential
ψ	dimensionless stream function, ψ'/α_f
Φ	dimensionless temperature, Eq. (??)
Ψ	dimensionless stream function, Eq. (??)

Superscripts

$'$	dimensional quantities
$*$	dimensionless variables, Eq. (??)
$\hat{}$	perturbation from the rest state

Subscripts

C	cold isothermal boundary
cr	critical value for the onset of convection
H	hot isothermal boundary
max	maximum value

Chapter 1

INTRODUCTION

Natural convection in a rectangular porous cavity heated from the side has received considerable attention in recent years because of its applications in many engineering areas. A number of studies analyzing this problem model the system as a two-dimensional layer framed by two horizontal adiabatic walls and two vertical isothermal walls. These studies have reported extensive theoretical [1], [2], [3], [4], numerical [5],[6],[7] and experimental [8], [9],[10] results with regard to the flow and heat transfer characteristics of the porous layer. The state-of-the art has been summarized in a recent book by Nield and Bejan [11].

Most of the existing studies are concerned with the natural convection heat transfer through a porous medium saturated by an electrically non-conducting fluid, which is the case in most practical situations. Recently, the equally important problem of hydromagnetic convective flow of a conducting fluid through a porous medium has been investigated. When an electrically conducting fluid is subjected to a magnetic field, the fluid motion induces an electric current and, in general, the fluid velocity is reduced due to interaction between the electric current and the motion. Very little has been done on the natural convection of electrically conducting fluids in porous media in the presence of a magnetic field in spite of its potential applications. For instance, the study of the interaction of the geomagnetic field with the fluid in the geothermal region, where the earth's crust

serves as a porous medium, is of great importance to geophysicists. Also, in metallurgical applications involving continuous casting, the solidification structure can be improved by electromagnetic stirring to obtain a fine-grained structure to get better final mechanical properties. For dendritic solidification of alloys, dendrites in the mushy zone can be viewed as a porous medium.

The interaction of an external magnetic field with convection currents in a porous medium was apparently first considered by Raptis et al. [12], [13]. They studied (Raptis et al. [12]) the influence of a horizontal constant magnetic field upon the free convective flow through a porous medium occupying a semi-infinite region of the space bounded by two vertical infinite surfaces. Raptis et al. [13] further extended their investigation to study the free convection flow of a conducting fluid through a porous medium bounded by two horizontal plates. Under the assumption that the magnetic Reynolds number is very small, so that the induced magnetic field can be considered negligible, closed form solutions were obtained for the velocity field in terms of the Grashof, permeability and magnetic parameters. Singh and Dikshit [14] studied the free convection of the Couette motion of an electrically conducting fluid through a porous medium. Exact solutions for the velocity field, skin-friction and the volume flux of the fluid were obtained in terms of the governing parameters of the problem. Kumar Jha and Prasad [15] studied the heat source characteristics on the free-convection and mass transfer flow past an impulsively started infinite vertical plate bounding a saturated porous medium under the action of a magnetic field. Effects of various parameters on the velocity field were extensively discussed. An analysis of the effects of Hall current on hydromagnetic free-convective flow through a porous medium bounded by a vertical

plate has been theoretically investigated by Takhar and Ram [16]. A strong magnetic field was imposed in a direction which is perpendicular to the free stream and makes an angle α to the vertical direction. The influence of Hall currents on the flow was studied for various values of α. Recently, Ni et al. [17] investigated the effect of an electromagnetic field on steady natural convection in a vertical enclosure filled with a porous medium. Numerical results in terms of velocity and temperature plots and Nusselt number distributions were discussed in order to understand the electromagnetic phenomena during the flow in porous media. It was demonstrated that for a large Hartmann number the electromagnetic field retards the flow in porous media just like a less permeable porous matrix.

In the present study, an investigation is conducted to examine the effect of an electromagnetic field on two dimensional natural convection in an inclined slot filled with an isotropic porous medium saturated by an electrically conducting fluid. The magnetic field is applied perpendicularly to the long side walls of the cavity which are differentially heated. In the special case of a vertical enclosure an analytical Oseen-linearized solution for the boundary-layer regime is presented. When the cavity is inclined the problem becomes more complicated and is studied through numerical simulations. The influences of the governing parameters on the fluid flow and heat transfer characteristics are well established.

Chapter 2

MATHEMATICAL MODEL

2.1 PROBLEM DISCRETIZATION

The physical model considered in this paper is shown in Fig. 1. A two-dimensional inclined rectangular enclosure of height H and width L is filled with a porous medium saturated by an electrically conducting fluid. The two long side walls are maintained at temperatures T'_H and T'_C respectively, while the short end walls are thermally insulated. A constant magnetic field $\vec{B}'$ is applied normal to the heated sides of the cavity. The fluid in this enclosure experiences the combined mechanism of buoyancy, due to heat transfer through the heated walls, and the interaction of the magnetic field with the convective motion. The magnetic Reynolds number is assumed to be small so that the induced magnetic field can be neglected compared to the applied magnetic field.

2.2 DIMENSIONAL GOVERNING EQUATIONS

The equations governing the conservation of mass, momentum, energy and electric charge transfer for laminar flow are written as

$$\nabla \cdot \vec{V}' = 0 \tag{2.1}$$

$$\frac{\mu}{K}\vec{V}' = -\nabla p' + \rho\vec{g} + \vec{J}' \times \vec{B}' \tag{2.2}$$

$$\vec{V}' \cdot \nabla T' = \alpha \nabla^2 T' \tag{2.3}$$

$$\nabla \cdot \vec{J'} = 0 \quad ; \quad \vec{J'} = \sigma(-\nabla\phi + \vec{V'} \times \vec{B'}) \tag{2.4}$$

These equations corespond to having the porous medium modeled according to the Darcy's law. The porous medium is assumed to be hydrodynamically, thermally and electrically isotropic and saturated with a fluid that is in local thermodynamic equilibrium with the solid matrix. Both viscous dissipation and Joulean energy dissipation are neglected.

In the above equations $\vec{V'}$, T' and p' are the intrinsic velocity, temperature and pressure of the fluid respectively. The terms $\vec{J'}$ and $\vec{B'}$ in the momentum equation are the intrinsic current vector and the magnetic field, respectively. The cross product of $\vec{J'}$ and $\vec{B'}$ represents the electromagnetic reduced momentum force, called the Lorentz force, on the liquid medium, which is produced by the interaction of the current and the magnetic field. The term ϕ stands for the electric potential and $-\nabla\phi$ for the associated electric field.

As discussed by Garandet et al. [18], for a two-dimensional steady state situation, Eq. (4) for the electric potential reduces to $\nabla^2\phi = 0$. The unique solution is $\nabla\phi = 0$ since there is always somewhere around the enclosure an electrically insulating boundary on which $\partial\phi/\partial n = 0$, which means that the electric field vanishes everywhere. The Lorentz force then reduces to a systematically damping factor.

In Eq. (2.4) $\vec{V'}$ and $\vec{B'}$ can be expressed as

$$\vec{V'} = (u', v', 0) \tag{2.5}$$

$$\vec{B'} = (B'_0, 0, 0) \tag{2.6}$$

then

$$\vec{V}' \times \vec{B}' = \begin{vmatrix} \vec{i} & \vec{j} & \vec{k} \\ u' & v' & 0 \\ B'_o & 0 & 0 \end{vmatrix} = -B'_0 v' \vec{k} \tag{2.7}$$

Substituting Eq. (2.7) into Eq. (2.4), we have

$$\begin{aligned} \vec{J}' &= \sigma(-\nabla\phi + \vec{V}' \times \vec{B}') \\ &= \sigma(\vec{V}' \times \vec{B}') \\ &= -\sigma B'_0 v' \vec{k} \\ &= (0, 0, -\sigma B'_0 v') \end{aligned} \tag{2.8}$$

In Eq. (2.2), the term $\vec{J}' \times \vec{B}'$ can be expressed as

$$\vec{J}' \times \vec{B}' = \begin{vmatrix} \vec{i} & \vec{j} & \vec{k} \\ 0 & 0 & -\sigma B'_0 v' \\ B'_o & 0 & 0 \end{vmatrix}$$

$$
\begin{aligned}
&= -B_0'(\sigma B_0' v')\vec{j} \\
&= -\sigma B_0'^2 v'\vec{j} \\
&= (0, -\sigma B_0'^2 v', 0)
\end{aligned}
\tag{2.9}
$$

Using the Boussinesq approximation:

$$\rho = \rho_0[\vec{1} - \beta(T' - T_C')] \tag{2.10}$$

Eq. (2.2) in x' direction can be expressed as

$$\frac{\mu}{K}u' = -\frac{\partial p'}{\partial x'} - \rho_0 g[1 - \beta(T' - T_C')]cos\theta \tag{2.11}$$

Eq. (2.2) in y' direction can be expressed as

$$\frac{\mu}{K}v' = -\frac{\partial p'}{\partial y'} - \rho_0 g[1 - \beta(T' - T_C')]sin\theta - \sigma B_0'^2 v' \tag{2.12}$$

The derivative of Eq. (2.11) with respect to y' yields

$$\frac{\mu}{K}\frac{\partial u'}{\partial y'} = -\frac{\partial^2 p'}{\partial x' \partial y'} + \rho_0 g\beta\frac{\partial T'}{\partial y'}cos\theta \tag{2.13}$$

While the derivative of Eq. (2.12) with respect to x' is

$$\frac{\mu}{K}\frac{\partial v'}{\partial x'} = -\frac{\partial^2 p'}{\partial x' \partial y'} + \rho_0 g\beta\frac{\partial T'}{\partial x'}sin\theta - \sigma B_0'^2\frac{\partial v'}{\partial x'} \tag{2.14}$$

Combining Eq. (2.13)−Eq. (2.14), we obtain

$$\frac{\mu}{K}\frac{\partial u'}{\partial y'} - (\frac{\mu}{K} + \sigma B_0'^2)\frac{\partial v'}{\partial x'} = -\rho_0 g\beta(\frac{\partial T'}{\partial x'}sin\theta - \frac{\partial T'}{\partial y'}cos\theta) \tag{2.15}$$

Due to the definition of velocity:

$$u' = \frac{\partial \psi'}{\partial y'} \quad ; \quad v' = -\frac{\partial \psi'}{\partial x'} \tag{2.16}$$

Substituting Eq. (2.16) into Eq. (2.15), the momentum equation can be written as

$$\frac{\mu}{K}\frac{\partial^2 \psi'}{\partial y'^2} + (\frac{\mu}{K} + \sigma B_0'^2)\frac{\partial^2 \psi'}{\partial x'^2} = -\rho_0 g\beta(\frac{\partial T'}{\partial x'}sin\theta - \frac{\partial T'}{\partial y'}cos\theta) \tag{2.17}$$

The continuity equation and energy equation can be writen as

$$\frac{\partial u'}{\partial x'} + \frac{\partial v'}{\partial y'} = 0 \tag{2.18}$$

$$u'\frac{\partial T'}{\partial x'} + v'\frac{\partial T'}{\partial y'} = \alpha(\frac{\partial^2 T'}{\partial x'^2} + \frac{\partial^2 T'}{\partial y'^2}) \tag{2.19}$$

The boundary condition of Eqs. (2.16–2.19) are

$$\begin{cases} \psi' = 0, \quad T' = T_C \quad on \quad x' = 0 \\ \psi' = 0, \quad T' = T_H \quad on \quad x' = L \\ \psi' = 0, \quad \dfrac{\partial T'}{\partial y'} = 0 \quad on \quad y' = \pm H/2 \end{cases} \tag{2.20}$$

2.3 DIMENSIONLESS GOVERNING EQUATIONS

Following dimensionless scales are used in the dimensional governing equations (2.16–2.19),

$$\begin{cases} x = \dfrac{x'}{L}; & y = \dfrac{y'}{L} \\ u = \dfrac{u'}{\alpha/L}; & v = \dfrac{v'}{\alpha/L} \\ \psi = \dfrac{\psi'}{\alpha}; & T = \dfrac{T' - T'_C}{T'_H - T'_C} \end{cases} \tag{2.21}$$

It is readily shown that the dimensionless governing equations can be expressed as

$$\frac{\partial u}{\partial x} + \frac{\partial v}{\partial y} = 0 \tag{2.22}$$

$$(1 + Ha^2)\frac{\partial^2 \psi}{\partial x^2} + \frac{\partial^2 \psi}{\partial y^2} = -R(\frac{\partial T}{\partial x} sin\theta - \frac{\partial T}{\partial y} cos\theta) \tag{2.23}$$

$$\nabla^2 T = \frac{\partial \psi}{\partial y}\frac{\partial T}{\partial x} - \frac{\partial \psi}{\partial x}\frac{\partial T}{\partial y} \tag{2.24}$$

where ψ is a dimensionless stream function defined as

$$u = \frac{\partial \psi}{\partial y} \quad ; \quad v = -\frac{\partial \psi}{\partial x} \tag{2.25}$$

In the above dimensionless equations the Darcy-Rayleigh number R and the Hartmann number Ha are

$$\begin{aligned} R &= Kg\beta L\Delta T'/\alpha_f \nu \\ Ha &= B'_0\sqrt{\sigma K/\mu} \end{aligned} \tag{2.26}$$

The non-dimensional boundary conditions over the walls of the enclosure are

$$\begin{cases} \psi = 0, \quad T = 0 \quad on \quad x = 0 \\ \psi = 0, \quad T = 1 \quad on \quad x = 1 \\ \psi = 0, \quad \dfrac{\partial T}{\partial y} = 0 \quad on \quad y = \pm A/2 \end{cases} \tag{2.27}$$

where $A = H/L$ is the cavity aspect ratio.

2.4 DEFINITION OF THE NUSSELT NUMBER

The overall heat transfer rate across the enclosure is expressed by the average Nusselt number defined as

$$\begin{aligned} Nu &= \frac{q'}{q'_c} \\ &= \frac{kH \int_0^{\mathrm{L}} \left.\dfrac{\partial T'}{\partial x'}\right|_{x'=0} dy'}{kH\Delta T'/L} \\ &= \frac{1}{A} \int_{-A/2}^{A/2} \left.\frac{\partial T}{\partial x}\right|_{x=0} dy \end{aligned} \tag{2.28}$$

The present problem is dependent on the parameters R, Ha, A and θ. Ranges of these physical parameters are selected to explore the effects of the magnetic field on natural convection in porous media.

Chapter 3

NUMERICAL APPROACH

This chapter will provide an overview of the role and nature of the numerical techniques in terms of control volume approaches. This will be followed by a detailed description of a well-tested numerical procedure that can handle the present problem as well as a wide variety of engineering problems.

The foregoing governing equations (2.22–2.25) can be considered as particular cases of the general differential equation

$$\underbrace{\nabla \cdot (\vec{v} f)}_{\text{convective term}} = \underbrace{\nabla \cdot (\nabla f)}_{\text{diffusive term}} \tag{3.1}$$

where f is the general dependent variable which can represent velocity component, temperature and mass fraction. When a particular meaning is associated with f, the expressions are to be obtained by comparing the actual conservation for the chosen variable with the general equation, Eq. (3.1).

3.1 DOMAIN DISCRETIZATION

The numerical method to be described here is based on the control-volume formulation proposed by Pantankar [19]. The discretization equations (which are the algebraic counterparts of the differential equations) are derived by integrating the governing differential equation over a small region called the control volume. Each control volume is associated with a discrete point at which the dependent variables such as streamfunction, velocity and temperature are to be calculated.

Figure 2 shows a rectangular calculation domain subdivided into control volumes. The dashed lines denote the faces of the control volumes; these lines are drawn parallel to the two coordinate directions x and y. The grid points are placed at the geometric centers of the control volumes. The filled circular dots in Fig. 2 represent these grid points, and the solid lines joining them are called the grid lines. A typical control volume around point P is shown shaded. The grid point P communicates with the four neighboring grid points through the four faces of the control volume. These points are denoted by E, W, N, and S, implying the east, west, north, and south directions with respect to the center point P. It can be seen from Fig. 2 that the grid lines are extended to the boundaries of the calculation domain, and additional boundary grid points are placed at the ends of the grid lines. Such grid points on the boundary are shown by open circles; B denotes a typical boundary grid point. A typical near-boundary internal grid point is shown as I, and its control volume is also shaded. For this control volume, one face coincides with the boundary of the calculation domain, and the boundary grid point B is placed at the center of this face. That both a control-volume face and a grid point are located at the boundary of the calculation domain makes it easy to treat different boundary conditions; the control volume around I can easily accept a given value of f at the boundary.

It is not necessary that the widths of all the control volumes be equal nor do the successive grid points have to maintain the same spacing between them. Indeed, a nonuniform grid spacing is often desirable, because it enables one to deploy a given number of grid points in an optimal manner. In general, a fine grid is required where the variation of f is steep, and a coarse grid is sufficient where

f varies rather slowly.

3.2 DISCRETIZATION OF THE GENERAL EQUATION

The basis of the numerical method is the conversion of the general differential equation, Eq. (3.1), into an algebraic equation relating the value of f at grid point P to the values at the neighboring grid points. This is done by integrating Eq. (3.1) over a typical control volume (Fig. 3) and approximating various terms in the integration so that they are expressed in terms of the grid-point value of f. The resulting discretization general equation becomes

$$a_P f_P = a_E f_E + a_W f_W + a_N f_N + a_S f_S + b \tag{3.2}$$

3.2.1 Discretization of the Momentum Equation

The momentum equation (2.23)

$$(1 + Ha^2)\frac{\partial^2 \psi}{\partial x^2} + \frac{\partial^2 \psi}{\partial y^2} = -R(\frac{\partial T}{\partial x} sin\theta - \frac{\partial T}{\partial y} cos\theta) \tag{3.3}$$

can be expressed as

$$\frac{\partial}{\partial x}\left[(1 + Ha^2)\frac{\partial \psi}{\partial x} + RT sin\theta\right] + \frac{\partial}{\partial y}\left[\frac{\partial \psi}{\partial y} - RT cos\theta\right] = 0 \tag{3.4}$$

or

$$\frac{\partial J_x}{\partial x} + \frac{\partial J_y}{\partial y} = 0 \tag{3.5}$$

where

$$\begin{aligned} J_x &= (1 + Ha^2)\frac{\partial \psi}{\partial x} + RT sin\theta \\ J_y &= \frac{\partial \psi}{\partial y} - RT cos\theta \end{aligned} \tag{3.6}$$

Integrating Eq. (3.5) over the control volume shown in Fig. 3, we obtain

$$J_e - J_w + J_n - J_s = 0 \tag{3.7}$$

where

$$\begin{aligned}
J_e &= \left[(1+Ha^2)\frac{\partial\psi}{\partial x} + RTsin\theta\right]\Big|_e \Delta y \\
&= \left[(1+Ha^2)\frac{\psi_E - \psi_P}{(\delta_x)_e} + \frac{1}{2}Rsin\theta(T_E + T_P)\right]\Delta y \\
J_w &= \left[(1+Ha^2)\frac{\partial\psi}{\partial x} + RTsin\theta\right]\Big|_w \Delta y \\
&= \left[(1+Ha^2)\frac{\psi_P - \psi_W}{(\delta_x)_w} + \frac{1}{2}Rsin\theta(T_P + T_W)\right]\Delta y \\
J_n &= \left[\frac{\partial\psi}{\partial y} - RTcos\theta\right]\Big|_n \Delta x \\
&= \left[\frac{\psi_N - \psi_P}{(\delta_y)_n} - \frac{1}{2}Rcos\theta(T_N + T_P)\right]\Delta x \\
J_s &= \left[\frac{\partial\psi}{\partial y} - RTcos\theta\right]\Big|_s \Delta x \\
&= \left[\frac{\psi_P - \psi_S}{(\delta_y)_s} - \frac{1}{2}Rcos\theta(T_P + T_S)\right]\Delta x
\end{aligned} \tag{3.8}$$

The resulting discretization momentum equation becomes

$$a_P\psi_P = a_E\psi_E + a_W\psi_W + a_N\psi_N + a_S\psi_S + b \tag{3.9}$$

where coefficients a_P, a_E, a_W, a_N, a_S and b are given by:

$$\begin{aligned} a_E &= \frac{(1+Ha^2)\Delta y}{(\delta_x)_e} \\ a_W &= \frac{(1+Ha^2)\Delta y}{(\delta_x)_w} \\ a_N &= \frac{\Delta x}{(\delta_y)_n} \\ a_S &= \frac{\Delta x}{(\delta_y)_s} \\ a_P &= a_E + a_W + a_N + a_S \\ b &= \frac{1}{2}R\left[(T_E sin\theta - T_W sin\theta)\Delta y - (T_N cos\theta + T_S cos\theta)\Delta x\right] \end{aligned} \tag{3.10}$$

3.2.2 Discretization of the Energy Equation

The energy equation (2.24) is

$$\frac{\partial^2 T}{\partial x^2} + \frac{\partial^2 T}{\partial y^2} = u\frac{\partial T}{\partial x} + v\frac{\partial T}{\partial y} \tag{3.11}$$

It can be rewriten as

$$\frac{\partial}{\partial x}\left(uT - \frac{\partial T}{\partial x}\right) + \frac{\partial}{\partial y}\left(vT - \frac{\partial T}{\partial y}\right) = 0 \tag{3.12}$$

or

$$\frac{\partial J_x}{\partial x} + \frac{\partial J_y}{\partial y} = 0 \tag{3.13}$$

where J_x and J_y are given by

$$\begin{aligned} J_x &= uT - \frac{\partial T}{\partial x} \\ J_y &= vT - \frac{\partial T}{\partial y} \end{aligned} \tag{3.14}$$

Integrating Eq. (3.13) over the contral volume shown in Fig. 3, we have

$$J_e - J_w + J_n - J_s = 0 \tag{3.15}$$

The continuty equation (2.22) is

$$\frac{\partial u}{\partial x} + \frac{\partial v}{\partial y} = 0 \tag{3.16}$$

Integrating the continuity equation over the control volume as

$$\int_s^n \int_w^e \left(\frac{\partial u}{\partial x} + \frac{\partial v}{\partial y} \right) dx dy = 0 \tag{3.17}$$

So, we have

$$u_e \Delta y - u_w \Delta y + u_n \Delta x - u_s \Delta x = 0 \tag{3.18}$$

It can be written as

$$F_e - F_w + F_n - F_s = 0 \tag{3.19}$$

where

$$\begin{aligned} F_e &= u_e \Delta y \\ F_w &= u_w \Delta y \\ F_n &= u_n \Delta x \\ F_s &= u_s \Delta x \end{aligned} \tag{3.20}$$

Mutiplying Eq. (3.19) by T_P, we have

$$F_e T_p - F_w T_p + F_n T_p - F_s T_p = 0 \tag{3.21}$$

From Eq. (3.15)–Eq. (3.21), we have

$$(J_e - F_e T_p) - (J_w - F_w T_p) + (J_n - F_n T_p) - (J_s - F_s T_p) = 0 \tag{3.22}$$

where

$$\begin{aligned} J_e - F_e T_p &= a_E(T_P - T_E) \\ J_w - F_w T_p &= a_W(T_W - T_P) \\ J_n - F_n T_p &= a_N(T_P - T_N) \\ J_s - F_s T_p &= a_S(T_S - T_P) \end{aligned} \tag{3.23}$$

The resulting discretization energy equation becomes

$$a_P T_P = a_E T_E + a_W T_W + a_N T_N + a_S T_S \tag{3.24}$$

where coefficients a_E, a_W, a_N, a_S and a_P are given by

$$\begin{aligned} a_E &= D_e A(|P_e|) + max(-F_e, 0) \\ a_W &= D_w A(|P_w|) + max(F_w, 0) \\ a_N &= D_n A(|P_n|) + max(-F_n, 0) \\ a_S &= D_s A(|P_s|) + max(F_s, 0) \\ a_P &= a_E + a_W + a_N + a_S \end{aligned} \tag{3.25}$$

where coefficients $D_e, D_w, D_n, D_s, P_e, P_w, P_n$ and P_s are given by

$$\begin{aligned} D_e &= \frac{\Delta y}{(\delta_x)_e} \\ D_w &= \frac{\Delta y}{(\delta_x)_w} \\ D_n &= \frac{\Delta x}{(\delta_y)_n} \\ D_s &= \frac{\Delta x}{(\delta_y)_s} \end{aligned} \tag{3.26}$$

$$\begin{aligned} P_e &= \frac{F_e}{D_e} \\ P_w &= \frac{F_w}{D_w} \\ P_n &= \frac{F_n}{D_n} \\ P_s &= \frac{F_s}{D_s} \end{aligned} \tag{3.27}$$

Table 3.1 The function $A(|P|)$ for different schemes

Scheme	Formula for $A(\|P\|)$
Central difference	$1 - 0.5\|P\|$
Upwind	1
Hybrid	$max(0.1 - 0.5\|P\|)$
Power law	$max(0, (1 - 0.1\|P\|)^5)$
Exponential	$\|P\|/[exp(\|P\|) - 1]$

The definition of $A(|P|)$ depends on the different choice of interpolation scheme for f calculation over the control volume considered. Expressions for $A(|P|)$ are listed in Table 3.1.

For the present work, we found that the power-law scheme provide an extremely good approximation.

3.2.3 Discretization of the Velocity

Based on the definition of velocity

$$u = \frac{\partial \psi}{\partial y} \quad ; \quad v = -\frac{\partial \psi}{\partial x} \tag{3.28}$$

the velocity u and v at the point P are given by

$$\begin{aligned} u_P &= \frac{(\delta_y)_s u_n + (\delta_y)_n u_s}{(\delta_y)_n + (\delta_y)_s} \\ v_P &= \frac{(\delta_x)_w v_e + (\delta_x)_e v_w}{(\delta_x)_e + (\delta_x)_w} \end{aligned} \tag{3.29}$$

where

$$\begin{aligned} u_n &= \frac{\psi_N - \psi_P}{(\delta_y)_n} \\ u_s &= \frac{\psi_P - \psi_S}{(\delta_y)_s} \\ v_e &= \frac{\psi_P - \psi_E}{(\delta_x)_e} \\ v_w &= \frac{\psi_W - \psi_P}{(\delta_x)_w} \end{aligned} \tag{3.30}$$

Numerical solutions of the full conservation equations are obtained using the control-volume finite difference method described by Patankar [19]. A power law

scheme is adopted for the convection-diffusion formulation. The discretized equations obtained are solved iteratively, using a line-by-line application of the Thomas algorithm. The numerical procedure starts with determining the temperature field T by solving the discretization energy equation (3.24). Next, the discretization momentum equation (3.9) is solved for ψ using a known temperature distribution. Finally, the velocity components are evaluated, for points that lie on the faces of each elementary control volume, using Eq. (3.29).

3.3 BOUNDARY CONDITIONS SETTING

With reference to Fig. 2, it can be seen that the grid is a control volume around each internal grid point of both temperature, stream function, and velocity components (u and v). We can write a corresponding discretization equation for this such as Eq.(3.2). This equation can be regarded as an equation for determining f_P. For a near-boundary control volume such as the one around grid point I in Fig. 2, the discretization equation will contain the boundary value f_B as one of the neighbors. If f_B is known, no additional information is needed.

If the $MX \times NY$ grids are used, we have boundary conditioins setting as below.

$$T(1,j) = 0, \qquad j = 1, \cdots, NY$$

$$T(MX,j) = 1, \qquad j = 1, \cdots, NY$$

$$T(i,2) = T(i,1), \qquad i = 2, \cdots, MX$$

$$T(i,NY-1) = T(i,NY), \quad i = 2, \cdots, MX$$

$$\begin{aligned}
&\psi(1,j) = 0, \qquad j = 1,\cdots,NY \\
&\psi(MX,j) = 0, \quad j = 1,\cdots,NY \\
&\psi(i,1) = 0, \qquad i = 1,\cdots,MX \\
&\psi(i,NY) = 0, \quad i = 1,\cdots,MX
\end{aligned} \tag{3.31}$$

At bounderay $i = 1$ or $i = MX$, $u = 0$. At bounderay $j = 1$ or $j = NY$, $v = 0$.

3.4 CALCULATION PROCEDURE

As indicated in the foregoing sections, the general calculation procedure is based on the solution of the general f equation. It should be mentioned here that it is in some sense necessary to use under-relaxation factor for the dependent variables and other auxiliary quantities to meet the requirement of convergence. Thus,

$$f = \alpha f_{\text{new}} + (1-\alpha) f_{\text{old}} \tag{3.32}$$

Of course, the value of α appearing in Eq.(3.32) need not be the same, nor is it necessary to use the same value of α for every grid point.

Although different forms of under-relaxation promote convergence, there is no unconditional guarantee that the iterative solution procedure will always converge for all kinds of nonlinearities and interlinkages. Also, there are no general formulas for choosing the optimum values of the under-relaxation factors. To

this extent, obtaining converged solutions for different problems remains an art. With sufficient experience and insight, one is normally able to devise an under-relaxation procedure that produces a converged solution. But a successful outcome may sometimes be preceded by an experience of divergence.

Prior to calculations, checks were conducted to validate the calculation procedure by reference to the flow of a vertical porous enclosure. In the limiting case of no magnetic field ($Ha = 0$), some of the cases considered by Shiralkar et al. [6] were reproduced. In general it was found that essentially identical flow and temperature patterns as well as Nusselt number were obtained. For instance when $R = 500$ and $A = 5.0$, an overall Nusselt number of 5.02 was obtained in the present study while that reported by Lauriat and Prasad [20] was 4.92. As an additional check on the accuracy of the results the convergence of the numerical solutions was checked by performing overall energy conservations.

Uniform mesh spacing was used in the x-direction and y-direction. Trial calculations were necessary in order to optimize computation time and accuracy. Convergence was verified by employing coarser and finer grids on selected test problems. During the program tests, 61×41, 61×61 and 81×81 grids were used. Because of minor differences (less than 1%) and to save on computation cost, the results presented here are obtained with 61×41 for a cavity with an aspect ratio $A = 4$ and 61×61 with $A = 8$. The criterion used for the iterative convergence is

$$max \frac{|f_{i,jnew} - f_{i,jold}|}{|f_{i,jold}|} < r_f \tag{3.33}$$

were $f_{i,j}$ stands for temperature and stream function and r_f has been taken as 10^{-4} for ψ and 10^{-6} for T.

Chapter 4

RESULTS AND DISCUSSION

In this section the results of the numerical study are discussed in order to understand the natural convection of an electrically conducting fluid in an inclined porous enclosure in the presence of a magnetic field. The non-dimensional parameters are the Rayleigh number R, the Hartmann number Ha, the aspect ratio A and the inclination angle θ. In the present study $A = 4$, 6 and 8. Computations are carried out for R ranging from 2×10^2 to 5×10^3, Ha ranging from 0 to 10 and $0^0 \leq \theta \leq 180^0$. Changes in the field characteristics due to combined effect of buoyancy and applied magnetic field are discussed in detail. Effects of the magnetic field on the average Nusselt number are also discussed. First, the case of a vertical cavity will be considered. Then, the case of a horizontal layer heated from below will be studied. Finally, we will investigate the influence of the inclination of the layer on the present problem.

4.1 VERTICAL LAYER HEATED FROM THE SIDES

We consider the influence of a magnetic field on flow and temperature distributions within a vertical enclosure ($\theta = 90^0$). Figures 4a-d show typical contour maps of stream function and temperature obtained numerically for $R = 500$, $A = 4$ and various values of Ha. In all these graphs the increments between adjacent streamlines and isotherms are $\delta\psi = \psi_{max}/10$ and $\delta T = 0.1$ where ψ_{max} is the maximum value of the stream function. The influence of a magnetic field

on flow and temperature distributions is apparent from these figures. In the absence of a magnetic field the flow and temperature fields of Fig. 4a are similar to the results obtained in the past by many investigators (see for instance Nield and Bejan [11]). Thus the flow field comprises a unicellular flow of relatively high velocity, circulating around the entire cavity. Due to boundary layer effects the temperature field is characterized by sharp drops in temperature near the vertical walls. It is interesting to note that, if the magnetic field is relatively strengthened the flow circulation is progressively inhibited by the retarding effect of the electromagnetic body force. Thus the maximum intensity of circulation is $\psi_{max} = 31.069$ for $Ha = 0$ but is only $\psi_{max} = 0.619$ for $Ha = 10$. For large Ha, Fig. 4d indicates that the convection is almost suppressed and the isotherms are nearly parallel to the vertical wall, indicating that a quasi-conduction regime is reached. Finally, it is observed from Fig. 4 that, although the thicknesses of the vertical boundary layers increase with Ha, the opposite effect is observed for the flow upon the horizontal walls. Thus, the flow pattern in Fig. 4d is characterized by a weak vertical flow but a very strong horizontal flow through very thin hydrodynamic boundary layers near the horizontal walls.

Figures 5 and 6 show the vertical velocity profiles and temperature profiles respectively at mid-height of the enclosure for $R = 500$, $A = 4$ and various values of Ha. In both graphs the results are presented only for $0 \leq x \leq 0.5$ due to the centro-symmetry of the problem. Since the porous medium has been modeled according to the Darcy's law the fluid is allowed to slip on the solid boundary, as indicated by Fig. 5, 6. In fact, independent of Ha, the fluid velocity is maximum on the wall and then drops back to zero in the core region of the cavity. The

suppression of the velocity held by the magnetic field is demonstrated in Fig. 5. It is clear that with the increase in Ha the vertical velocity is considerably decreased, specially in the vicinity of the solid wall. The effect of Ha on temperature profiles is depicted on Fig. 6. In the absence of a magnetic drag ($Ha = 0$), the convective motion within the cavity is maximum since the only resistance to the flow within the porous media is due to the presence of the solid matrix. A maximum quantity of heat is extracted from the wall as indicated by the relatively high temperature gradient prevailing in this area. However, as the strength of the magnetic field is progressively increased the retarding effect caused by the Lorentz's force becomes gradually more important and adds to the bulk frictional drag induced by the solid matrix to slow down the convective motion. As a result relatively less heat is removed from the wall where the temperature gradient decreases accordingly. Thus, for $Ha = 3$, convection has been almost completely damped by the magnetic field (see Fig. 5) and the resulting temperature distribution is now very close to the pure conduction regime shown as a dotted line in Fig. 6.

In general, the quantities of interest involved in the present problem are related in so complicated a way that would not allow estimations of their orders of magnitudes by a scale analysis. However, for a vertical cavity, for the limiting case of boundary layer flow regime, an order of magnitude estimates can be derived on scaling grounds.

In the boundary layer regime, i.e., when $R >> 1$, most of the fluid motion is restricted to a thin layer δ' along each vertical wall. Recognizing δ' and H as the x' and y' scales in the boundary layer region of interest ($\delta' << H$) the conservation

equations (2.23) and (2.24) require the following balances

$$(1 + Ha^2)\frac{v}{\delta} \sim R\frac{\Delta T}{\delta} \tag{4.1}$$

$$v\frac{\Delta T}{A} \sim \frac{\Delta T}{\delta^2} \tag{4.2}$$

where $\delta = (\delta'/H)$ is the dimensionless thickness of the horizontal boundary layer, and ΔT is the dimensionless temperature difference across the boundary layer. Obviously, from the thermal boundary conditions, Eqs. (2.27), $\Delta T \sim 1$.

Solving the balance equations for v and δ one obtains

$$\delta \sim [A(1 + Ha^2)/R]^{1/2} \tag{4.3}$$

$$v \sim R/(1 + Ha^2) \tag{4.4}$$

The order of magnitude of the velocity component u is obtained from the continuity equation (2.22) as

$$u \sim \frac{v\delta}{A} \sim [R/(A(1 + Ha^2))]^{1/2} \tag{4.5}$$

The scale for the stream function can be obtained from Eq. (2.25) as

$$\psi \sim [RA/(1 + Ha^2)]^{1/2} \tag{4.6}$$

The total heat transfer rate from one side wall to the other is given by

$$q' \sim kH\frac{\Delta T'}{\delta'} \tag{4.7}$$

The average Nusselt number, defined as the total heat transfer over the pure heat conduction through the cavity, has the following scale

$$Nu = \frac{q'}{q'_c} = \frac{kH\Delta T'/\delta'}{kH\Delta T'/L} \sim \frac{1}{A^{1/2}} \frac{R^{1/2}}{(1+Ha^2)^{1/2}} \tag{4.8}$$

in which $q'_c = kH\Delta T'/L$ is the heat transfer in the pure-conduction limit.

In the absence of a magnetic field ($Ha = 0$) the above scales reduce to those predicted by Bejan [21] while studying the boundary layer regime within a porous cavity heated isothermally from the sides. The above results are expected to be valid only when the vertical boundary layers are slender ($\delta' << H$), i.e., for $R/(1+Ha^2) >> 1$. Also, the vertical boundary layers must be distinct ($\delta' << L$) which requires that $[R/(1+Ha^2)]^{1/2} >> A^{1/2}$.

The boundary-layer approximations to the governing equations can now be obtained from the results of the above order of magnitude analysis. When the following dimensionless variables are used

$$\begin{cases} x^* = \dfrac{x'}{l} & y^* = \dfrac{y'}{H} & \psi^* = \dfrac{\psi'}{\alpha_f}\dfrac{l}{L} \\ u^* = \dfrac{u'lA}{\alpha_f} & v^* = \dfrac{v'l^2}{\alpha_f L} & T^* = \dfrac{T'-T_c}{\Delta T'} \\ l^2 = \dfrac{LH}{R/(1+Ha^2)} & & \end{cases} \tag{4.9}$$

the approximate forms of Eqs. 2.23 and 2.24 can be obtained as

$$\frac{\partial v^*}{\partial x^*} = \frac{\partial T^*}{\partial x^*} \tag{4.10}$$

$$u^* \frac{\partial T^*}{\partial x^*} + v^* \frac{\partial T^*}{\partial y^*} = \frac{\partial^2 T^*}{\partial x^{*2}} \tag{4.11}$$

Defining the boundary-layer variables as (Gill, [22])

$$\begin{cases} T^* = T_0(y^*) + \Phi(x^*, y^*) \\ \psi^* = \psi_0(y^*) + \Psi(x^*, y^*) \end{cases} \tag{4.12}$$

where Φ and $\Psi \to 0$ as $x^* \to \infty$, we can establish the necessary boundary conditions

$$\begin{cases} at \quad x^* = 0, \quad \psi^* = 0 \qquad T^* = 0 \\ at \quad x^* \to \infty, \quad \psi^* = \psi_0(y^*) \quad T^* = T_0(y^*) \end{cases} \tag{4.13}$$

In the above equations $\psi_0(y^*)$ and $T_0(y^*)$ are the dimensionless stream function and temperature distribution within the core of the cavity.

The dimensionless nonlinear governing equations (4.10)–(4.11) and the boundary conditions (4.13) are exactly the same as those derived by Weber [1] and Simpkins and Blythe [4] while studying boundary layer flows within a porous layer in the absence of a magnetic field ($Ha = 0$). The analytical results obtained by Simpkins and Blythe [4], on the basis of an integral relation approach, will be used here since they proved to be in excellent agreement with numerical solutions of the boundary layer equations. Translating their results in our notation it is readily found that, for the present problem, the average Nusselt number is given by

$$Nu = 0.51[\frac{R}{A(1 + Ha^2)}]^{1/2} \tag{4.14}$$

Figure 7 shows the dependence of the Nusselt number Nu on the Rayleigh and Hartmann numbers. Results are presented for $5 \times 10^2 \leq R \leq 5 \times 10^3$ for

which a boundary layer flow regime prevails. The analytical results, Eq. (4.14), are continuous lines; numerical results obtained for $A = 4$ and 8, shown as solid symbols, are seen to agree well. In the absence of a magnetic field, Eq. (4.14) reduces to $Nu = 0.51\ (R/A)^{1/2}$ as predicted by Simpkins and Blythe [4]. For this situation, the numerical results obtained in the past by Lauriat and Prasad [20] for $A = 5$ are also indicated in the graph for comparison.

Another view of the effect of Ha on the heat transfer is found in Fig. 8 where Nu is plotted as a function of Ha for $R = 200$, 500 and 1500. The numerical results, obtained for $A = 4$, are depicted by the solid lines while the dotted lines represent the boundary layer regime, Eq. (4.14). For a given Rayleigh number, when Ha is relatively small, the flow is in the boundary layer regime and the numerically predicted Nusselt number is in good agreement with the analytical solution. The boundary layer regime prevails up to a given value of Ha above which this regime ends due to the progressively retarding effect of the electromagnetic body force. As the value of Ha is made larger the strength of the convective motion is progressively suppressed and the boundary layer regime is followed by the asymptotic and conduction regime for which $Nu \rightarrow 1$. Naturally, the Hartmann number ranges for asymptotic and conduction regimes are also extended as R is made larger.

4.2 HORIZONTAL LAYER HEATED FROM BELOW

The effect of a magnetic field on the Benard convection in a horizontal layer heated from below ($\theta = 180^0$) will be now considered. For this situation there is a critical Rayleigh number below which the fluid is at rest and heat transfer is by

pure conduction only. Since we have not found in the literature a linear stability analysis of the influence of a magnetic field on the Benard flow within an infinite horizontal porous layer heated from below we include a brief outline here. The problem is self adjoint so that the principle of exchange of stability holds. Thus, the time derivative in the governing equations does not need to be considered. The linearized local form of Eqs. (2.23)-(2.25) for small perturbations about the conductive state are

$$a\frac{\partial^2 \hat{u}}{\partial x^2} + \frac{\partial^2 \hat{u}}{\partial y^2} = -R\frac{\partial^2 \hat{T}}{\partial y^2} \tag{4.15}$$

$$\nabla^2 \hat{T} = \hat{u} \tag{4.16}$$

where the superscript $\hat{}$ indicates perturbations from the pure conduction state and $a = (1 + Ha^2)$. The above equations must satisfy the following boundary conditions:

$$\hat{u} = \hat{T} = 0 \quad at \quad x = 0, 1 \tag{4.17}$$

The solution to Eqs. (4.15)-(4.17) is obtained by assuming that

$$\hat{u} = U(x)e^{i\alpha y} \quad \hat{T} = T(x)e^{i\alpha y} \tag{4.18}$$

Substitution of Eq. (4.18) into Eqs. (4.15) and (4.16) and eliminating U from the resulting equations we obtain

$$a\theta^{IV} - \alpha^2(a+1)\theta^{II} + \alpha^4\theta = R\alpha^2\theta \tag{4.19}$$

This equation admits solutions of the form $\theta = Csin(n\pi y)$ where C is an arbitrary constant and n an integer so that the boundary condition, Eq. (4.17), is satisfied.

Substituting θ into Eq. (4.19) it is readily found that the assumed flow is neutrally stable when

$$R_{cr} = \frac{an^4\pi^4 + \alpha^2(a+1)n^2\pi^2 + \alpha^4}{\alpha^2} \tag{4.20}$$

so that the minimum value occurs at $n = 1$ and $\partial R_{cr}/\partial\alpha = 0$, that is, when

$$R_{cr} = \left(1 + \sqrt{Ha^2 + 1}\ \right)^2 \pi^2 \quad , \quad (n = 1, \quad \alpha = \pi(Ha^2+1)^{1/4}) \tag{4.21}$$

In the absence of a magnetic field, i.e., when $Ha = 0$, the above results reduce to

$$R_{cr} = 4\pi^2 \quad , \quad (n = 1, \alpha = \pi) \tag{4.22}$$

which are the classical results obtained in the past by Lapwood [23]. Figures 9a-d show typical streamlines and isotherms obtained numerically for $A = 6$, $R = 500$ and various values of Ha. In the absence of a magnetic field, i.e., when $Ha = 0$, it is seen from Fig. 9a that six cells of approximately equal size and intensity occupy the width of the porous layer. The shape of the cells is observed to be skewed by the strong convection, $\psi_{max} = 15.40$, resulting from a relatively high R considered here. The large distortion of the isotherms in Fig. 9a is also an indicator of the intensity of the convection within the fluid layer. A step increase in the strength of a magnetic field from $Ha = 0$ to 4 results in the response as shown in Fig. 9b. The six-cells mode obtained for $Ha = 0$ is now replaced by a eight-cells pattern. This trend is in agreement with the linear-stability theory, Eq. (4.21), according to which the effect of the magnetic field is to decrease the wavelength of the incipient cells ($\alpha = \pi(Ha^2+1)^{1/4}$). Also, the strength of convection is considerably decreased by the drag induced by the magnetic field, as indicated by

a weak distortion of the isothermal lines and the value of the maximum stream function which is now only $\psi_{max} = 3.03$. As the Hartmann number is further increased, up to $Ha = 5$, ten-cells of approximately equal size and intensity are seen to occupy now the width of the cavity. For this situation the isotherms of Fig. 9d indicates that the convective regime is very weak. In fact this situation is very close to the purely diffusive regime which, in an infinite porous layer, would occur according to Eq. (4.21) when $Ha \geq 6$ and $R = 500$.

Figure 10 presents relationship between the average Nusselt number and the Hartmann number for the case with $A = 6$ and $R = 500$. Naturally the heat transfer is maximum in the absence of a magnetic field since the convection is maximum for this situation. In general, Nu decreases steeply with the imposition of an external magnetic field since this latter reduces considerably, as discussed earlier, the strength of convection. At $Ha \simeq 3.6$, a slight increase of Nu is observed which results from the transition in the number of cells within the cavity from six to eight. At $Ha \simeq 4.5$ another bifurcation from a eight-cell to a ten-cell pattern occurs. Afterwards, the convective motion is more and more inhibited by the magnetic drag. At $Ha \simeq 5.0$ a bifurcation from a ten-cell to a twelve-cell pattern occurs, but the convection is now so low ($Nu \sim 1$) that it does not affect the heat transfer.

4.3 INCLINED CAVITY

The effect of a magnetic field on the natural convection heat transfer within a tilted cavity will be now discussed. This problem, in the absence of a magnetic field, has been considered recently by Caltagirone and Bories [24] and Moya et

al. [25]. It was demonstrated by these authors that, at tilt angles close to zero, the preferred mode of circulation is multiple cell while at greater tilt angles, the preferred mode is single cell. The transition angle from multiple to single cell convection patterns was shown to depend on the aspect ratio and the Rayleigh number. This phenomenon is illustrated in Figs. 11-13 where the streamlines are shown for $A = 4$, $R = 500$ and various values of the inclination angle θ. When the cavity is horizontal ($\theta = 180^0$) Fig. 11a shows that four cells develop with alternate directions of rotation (Benard's cells). As the inclination angle θ is decreased to 175^0 a five cell convection is obtained as illustrated by Fig. 11b. At this stage a remark must be made with regard to the numerical procedure followed here. In order to speed up the computational procedure the converged velocity and temperature fields, obtained from a numerical run with a given inclination angle θ, were used as initial conditions for another run with a small change in the tilt angle. In this way it was found that the five cell convection prevails (Fig. 11c,d) up to $\theta > 140^0$. For smaller tilt angles an evolution from multiple cells to single cell convection is observed. Thus, for $\theta = 140^0$, the flow in Fig. 11e is characterized by a single cell where all the fluid inside the porous material circulates in the same sense and the streamfunction has only one extremum value.

In the transitional region between multiple and single cell convection, flow hysteresis effects were observed in the present study. Thus, when the inclination angle increased from $\theta = 140^0$ back to $\theta = 180^0$ the flow field did not revert to the previous solutions for the same θ. For instance, the single cell solution observed for $\theta = 140^0$ could be maintained up to $\theta = 170^0$. Increasing θ to 171^0 it is found that the flow consists now of one main cell with secondary cells developing within.

This type of flow pattern, illustrated in Fig. 12a, has been observed in the past by Moya et al. [25]. As the tilt angle is increased further three cells develop with alternate directions of rotation and are maintained up to $\theta = 180^0$ (Fig. 12b). Similar phenomena have been observed on various values of Ha (Fig. 14-17). It is noted that, this flow "hysteresis" has not been observed in the past. In addition, the flow pattern change is slower with increasing Ha. Fig. 13 shows the patterns of isothermal lines and streamfunction of $Ha = 3$ with increasing the tilt angle up to $\theta = 180^0$.

The average Nusselt number Nu and maximum streamfunction ψ_{max} for aspect ratio of four and for several Hartmann numbers is shown in Figs. 14, 15 as a function of the tilt angle. As the inclination θ approaches 0^0 the Nusselt number tends toward unity, indicating that the heat transfer is mainly due to conduction. This is expected since $\theta = 0^0$ corresponds to the case of a cavity heated from the top which causes no convection as the density gradient is stable. Most of the change in the heat transfer occurs in the range $0^0 < \theta < 90^0$ where the cavity is heated from the top. Also, it is observed that, for a given inclination angle, the Nusselt number decreases with an increase of the Hartmann number since the convection is considerably decreased with the application of the magnetic field. As the inclination angle is increased above 90^0, the enclosure starts to be heated from the bottom. Each curve passes through a maximum which depends upon Ha. As demonstrated by Moya et al. [25] the peak in Nusselt number occurs approximately at an inclination angle for which the most vigorous convection flow is developed. As the inclination angle is increased further the curves are seen to pass through a second maximum. Contrary to the case of the first maximum

which was obtained for a single cell mode, the second maximum is due to the appearance of a multiple cell convection. The transition angle from single to multiple cell convection patterns depends strongly upon the magnetic field. For instance, a transition from one-cell to three-cell pattern occurs at $\theta = 171^0$ when $Ha = 0$ but it is at about $\theta = 141^0$ when $Ha = 1.7$. Therefore, the second peak in Nusselt number takes place at a lower transition angle when the Hartmann number is increased. Also, Fig. 14 indicates that, for $Ha = 3$, not only there is a transition from one-cell to three-cell pattern at $\theta \simeq 131^0$ but a second transition from three-cell to five-cell pattern occurs at $\theta \simeq 143^0$. Naturally, due to the flow hysteresis discussed before, the transition angles obtained when the inclination angle is decreased from $\theta = 180^0$ towards 0^0 are different from those of Fig. 14. From the numerical results (not presented here) it was found that the transition from multiple to single cell convection occurred in general at lower angles. For instance, when $Ha = 0$, a transition angle $\theta \simeq 140^0$ was obtained. Finally, it must be mentioned that the occurrence of the first maximum, for the single cell mode, was not affected by the hysteresis effect.

Figures 16 and 17 show the average Nusselt number Nu and maximum streamfunction ψ_{max} respectively for aspect ratio of four and for several Hartmann numbers with decreasing tilt angle from $\theta = 180^0$ to $\theta = 0^0$.

Chapter 5

CONCLUSIONS

The effect of a transverse magnetic field on buoyancy driven convection in an inclined rectangular porous cavity, saturated with an electrically conducting fluid, is studied both numerically and analytically. Main conclusions of this study are summarized as follows:

1^o In the case of a vertical cavity heated from the side ($\theta = 90^0$) it is shown that a simple dimensional analysis can predict correctly the asymptotic behaviour of the velocity field in the limit $R \rightarrow \infty$. Also, in the boundary layer regime, the dependence of the Nusselt number on R, A and Ha is obtained explicitly following the integral approach of Simpkins and Blythe [4]. The resulting expression, $Nu = 0.51[R/A(1+Ha^2)]^{1/2}$ was confirmed by comparing the numerical results obtained for cavities with aspect ratios $A = 4$ and 8.

2^o The effect of a magnetic field on the Benard convection, within a porous layer heated from below $\theta = 180^0$ has been considered. The critical Rayleigh number for the onset of convection has been predicted, using a linear stability theory. For supercritical convection, the adjustement of the roll pattern, after a change in the Hartmann number, is illustrated for a given Rayleigh number and a cavity with an aspect ratio $A = 6$. Results for the heat transfer as a function of Ha are presented.

3^o The effect of the orientation angle on the present problem was found

to be considerable. The transition angle from single cell to multiple convection pattern is considerably affected by the imposition of a magnetic field. Thus for a cavity with $R = 500$ and $A = 4$ the transition angle is $\theta = 171^0$ when $Ha = 0$ but it is $\theta = 131^0$ when $Ha = 3.0$.

Bibliography

[1] WEBER, J. W., The boundary layer regime for convection in a vertical porous layer. *Int. J. Heat Mass Transfer*, 18:569 –573, 1975.

[2] BEJAN, A. and TIEN, C. L., Natural convection in a horizontal porous medium subjected to an end-to-end temperature difference. *J. Heat Transfer*, 100:191 –198, 1978.

[3] WALKER, K. L. and HOMSY, G. M., Convection in a porous cavity. *J. Fluid Mech.*, 87:449 –474, 1978.

[4] SIMPKINS, P. G. and BLYTHE, P. A., Convection in a porous layer. *Int. J. Heat Mass Transfer*, 23:881 –887, 1980.

[5] HICKOX, C. B. and GARTLING, D.K., A numerical study of natural convection in a horizontal porous layer subjected to an end-to end temperature difference. *J. Heat Transfer*, 103:797 –802, 1981.

[6] SHIRALKAR, G. S., HAAJIZADEH, M. and TIEN. C L., Numerical study of high rayleigh number convection in a vertical porous enclosure. *Numerical Heat Transfer*, 6:223 –234, 1983.

[7] PRASAD, V. and KULACKI, F. A., Convective heat transfer in a rectangular porous cavity-effect of aspect ratio on flow structure and heat transfer. *J. Heat Transfer*, 106:158 –165, 1984.

[8] KLARSFELD, S., Champs de température associés aux mouvements de convection naturelle dans un milieu poreux limité. *Rev. Gen. Thermique*, 108:1403 –1432, 1970.

[9] MORDCHELLES-REGNIER, G., MICHEAU, P., PRIOVANO, A. JUMENTIER, C., TERPSTA, J.S., LECOURT, Y., CAVE, P. and BREUILLE, M., Recherches recentes effectuées en France sur l'isolation thermique des réacteurs nucléaires. In *International Atomic Energy Agency, Vienna*, 1969.

[10] SEKI, N., FUKUSAKO, S. and INABA, H., Heat transfer in a confined rectangular cavity packed with porous media. *Int. J. Heat Mass Transfer*, 106:152 –157, 1978.

[11] NIELD, D. A. and BEJAN, A., *Convection in Porous Media.* Springer-Verlag, 1992.

[12] RAPTIS, A., MASSALAS, C. and TZIVANIDIS, G., Hydromagnetic free convection flow through a porous medium between two parallel plates. *Physics Letters*, 90A:288 –289, 1982.

[13] RAPTIS, A. and VLAHOS, J., Unsteady hydromagnetic free convective flow through a porous medium. *Letters in Heat and Mass Transfer*, 9:56 –64, 1982.

[14] SINGH, A. K. and DIKSHIT, C. K., Natural convection effects of hydromagnetic generalised couette flow in a porous medium. *Indian J. Theoretical Physics*, 35:331 –335, 1987.

[15] KUMAR JHA, B. and PRASAD, R., MHD free-convection and mass transfer flow through a porous medium with heat source. *Astrophysics and Space Science*, 8:117 –123, 1991.

[16] TAKHAR, H. S. and RAM, P. C., Effects of hall current of hydromagnetic free-convective flow through a porous medium. *Astrophysics and Space Science*, 192:45 –51, 1992.

[17] NI, J., BECKERMANN, C. and SMITH, T. F., Effect of an electromagnetic field on natural convection in porous media. *Fundamentals of Heat Transfer in Electromagnetic, Electrostatic and Acoustic Fields, ASME*, 248:23 –33, 1993.

[18] GARANDET, J. P., ALBOUSSIERE, T. and MOREAU, R., Buoyancy driven convection in a rectangular enclosure with a transverse magnetic field. *Int. J. Heat Mass Transfer*, 35:741 –748, 1992.

[19] PATANKAR, S. V., *Numerical Heat Transfer and Fluid Flow.* Hemisphere Publishing Corp., 1980.

[20] LAURIAT, G. and PRASAD. V., Natural convection in a vertical porous cavity: a numerical study for Brinkman-extended Darcy formulation. *J. Heat Transfer*, 109:688 – 696, 1987.

[21] BEJAN, A., The method of scale analysis: Natural convection in a porous media. In *Natural Convection Fundamentals and Applications (ed S. Kalac et al.), Hemisphere, Washington, DC.*, 1985.

[22] GILL, A. E., The boundary-layer regime for convection in a rectangular cavity. *J. Fluid Mech.*, 26:515 –536, 1966.

[23] LAPWOOD, E. R., Convection of a fluid in a porous medium. *Proc. Cambridge Philos. Soc.*, 44:508 –521, 1948.

[24] CALTAGIRONE, J. P. and BORIES, S., Solutions and stability criteria of natural convection flow in an inclined porous layer. *J. Fluid Mech.*, 155:267 –287, 1985.

[25] MOYA, S. L., RAMOS, E. and SEN, M., Numerical study of natural convection in a tilted rectangular porous material. *Int. J. Heat Mass Transfer*, 30:741 –756, 1987.

Annexe

FIGURES

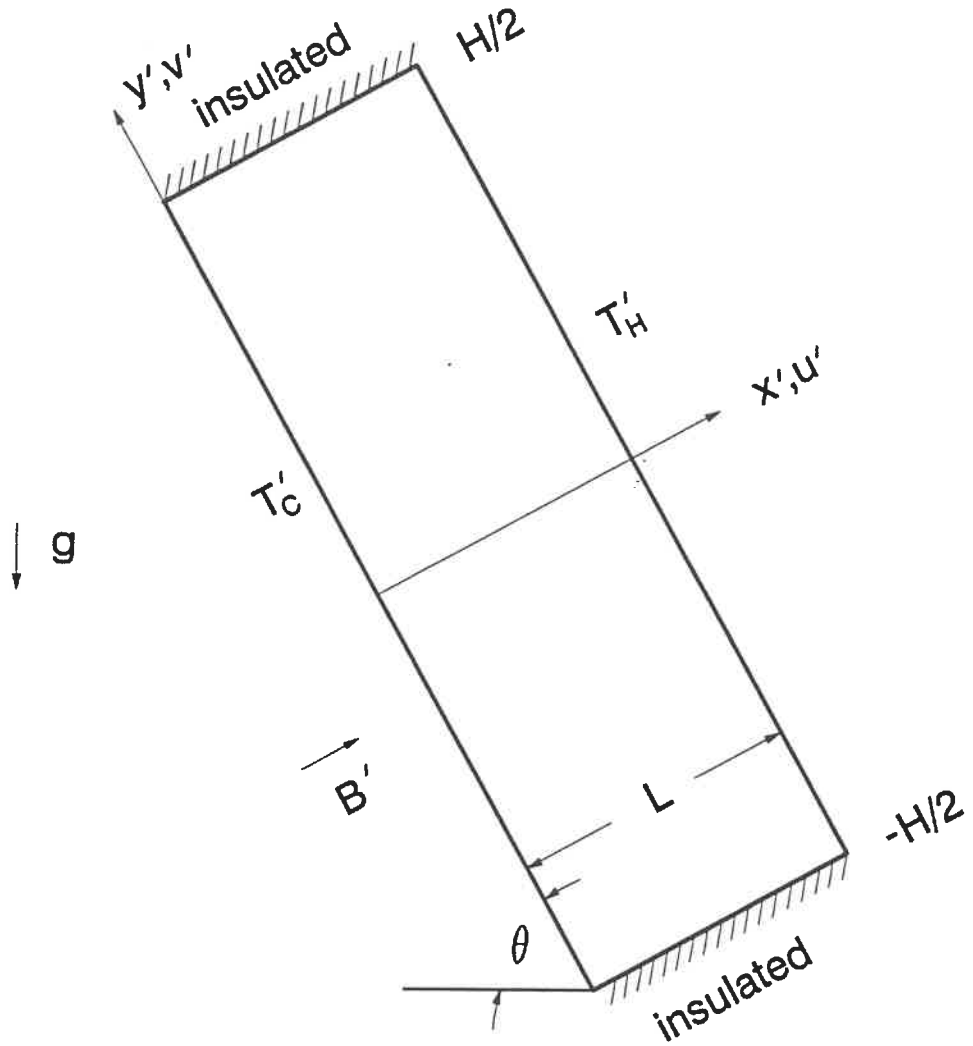

Fig. 1 Schematic of the problem

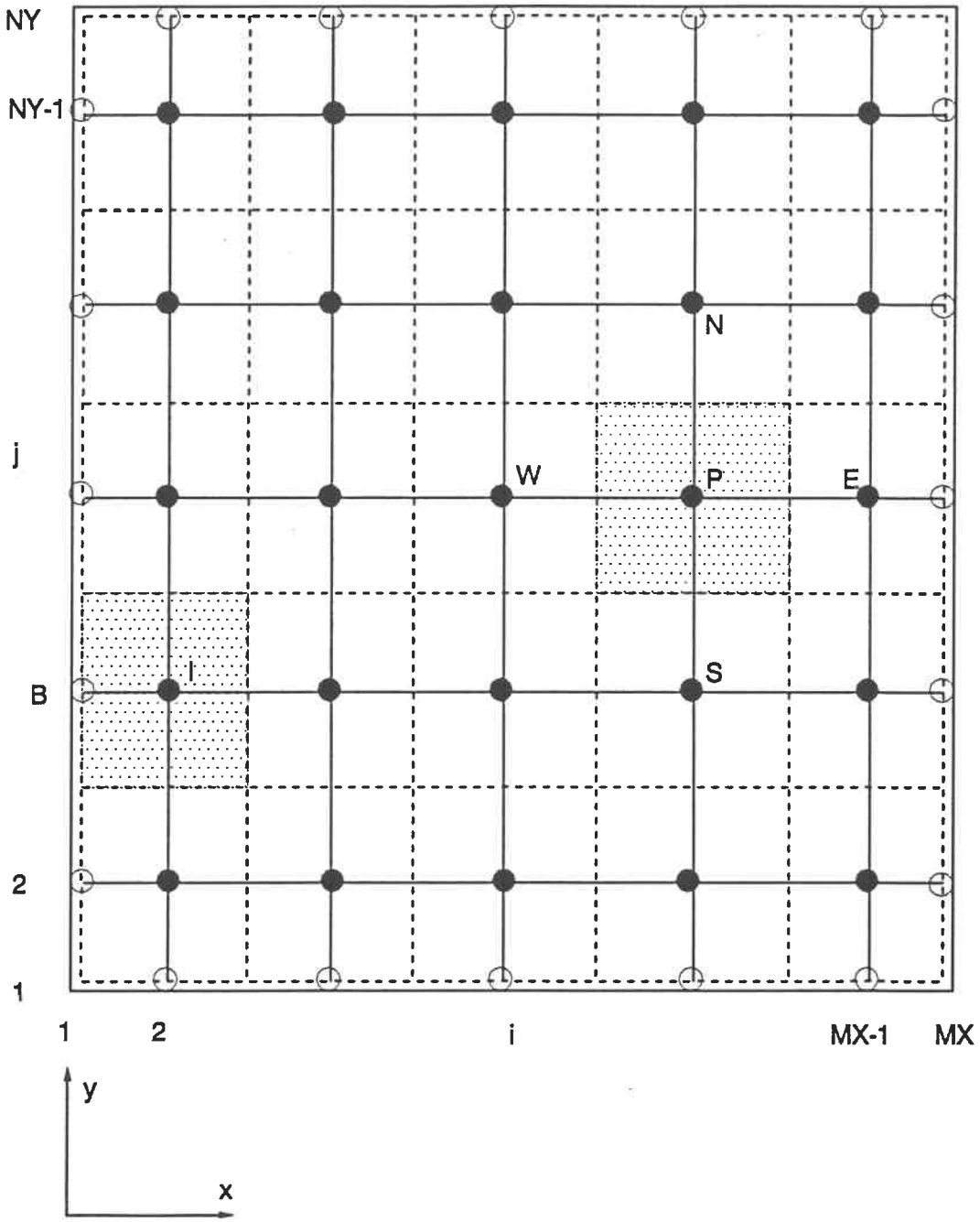

Fig. 2 Grids and control volumes

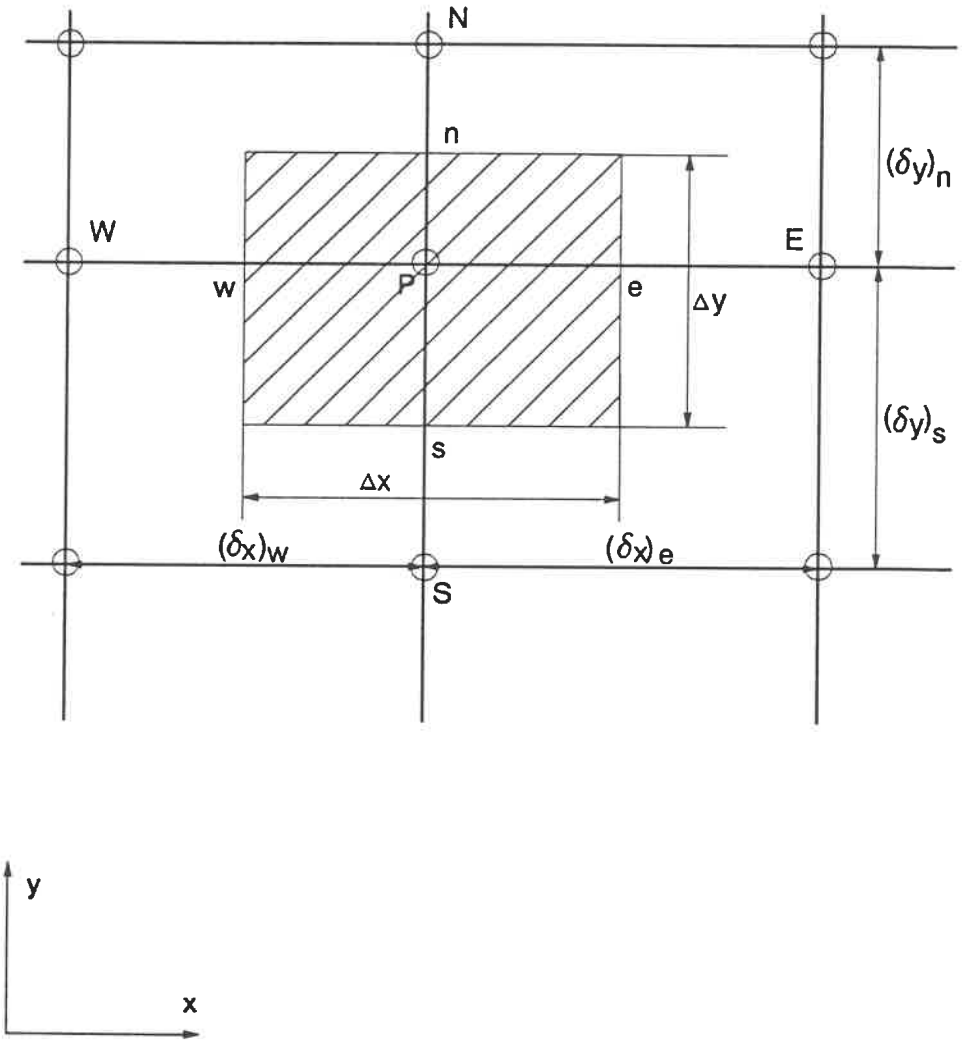

Fig. 3 A typical control volume

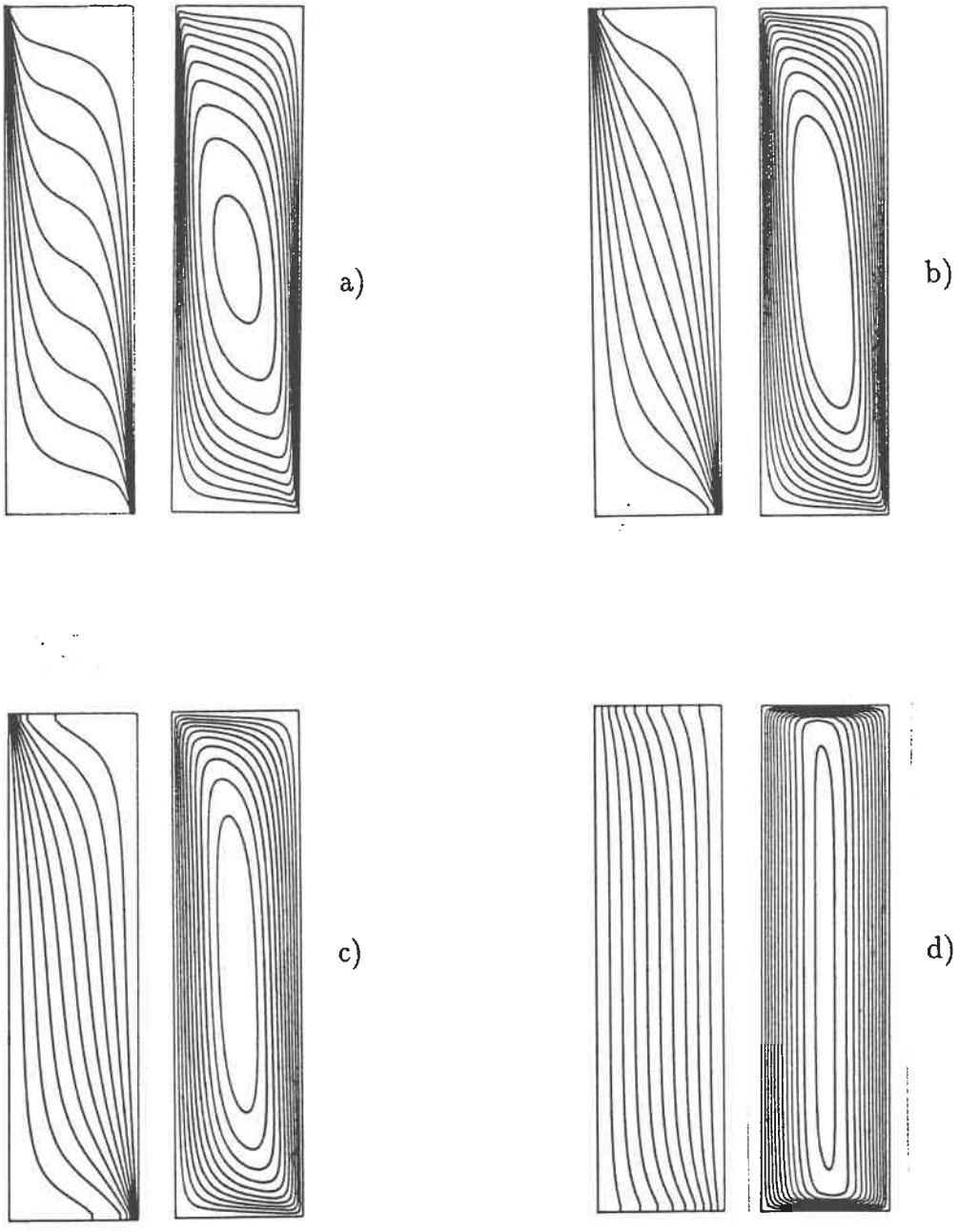

Fig. 4 Computed contour maps of the streamfunction and isothermal lines

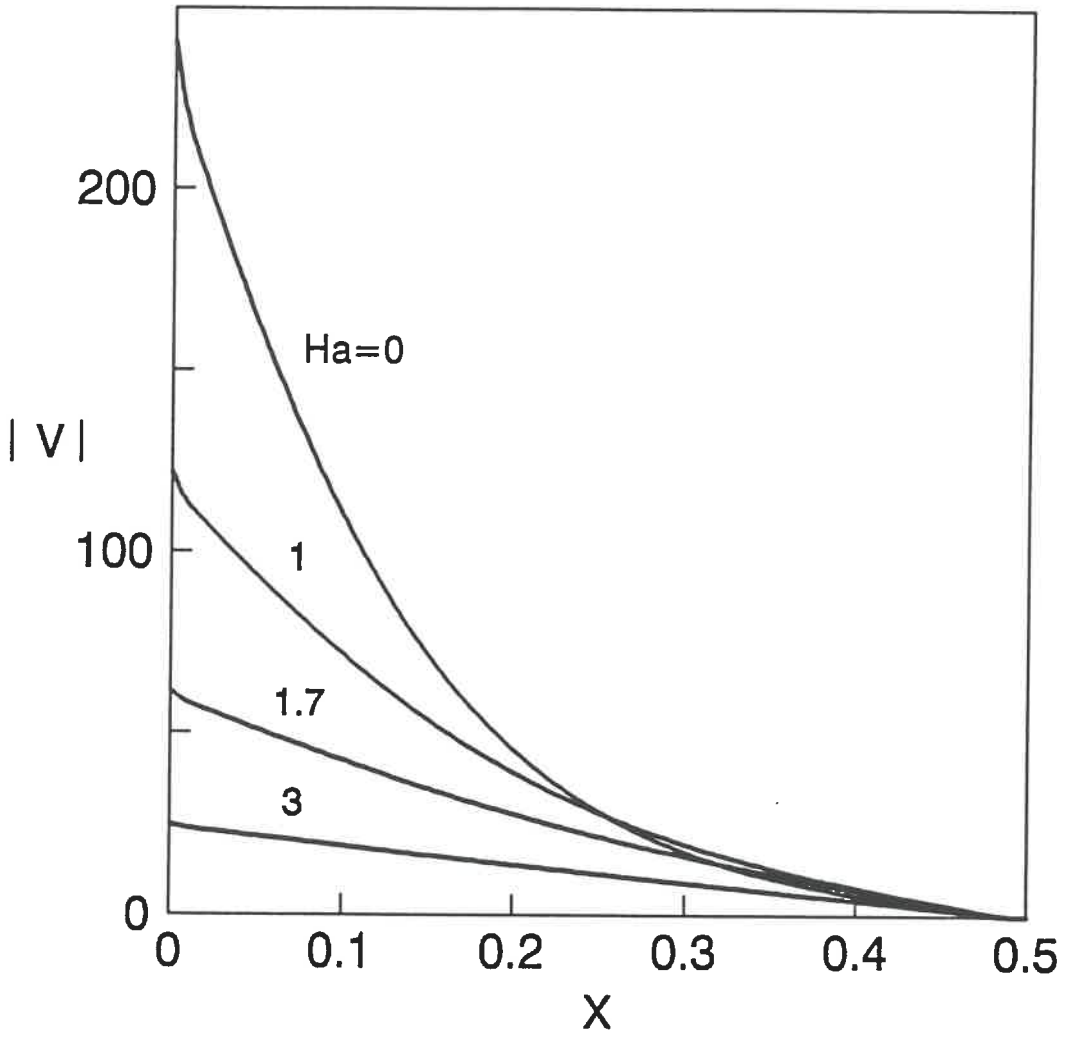

Fig. 5 The velocity profiles at mid-height of the cavity as a function

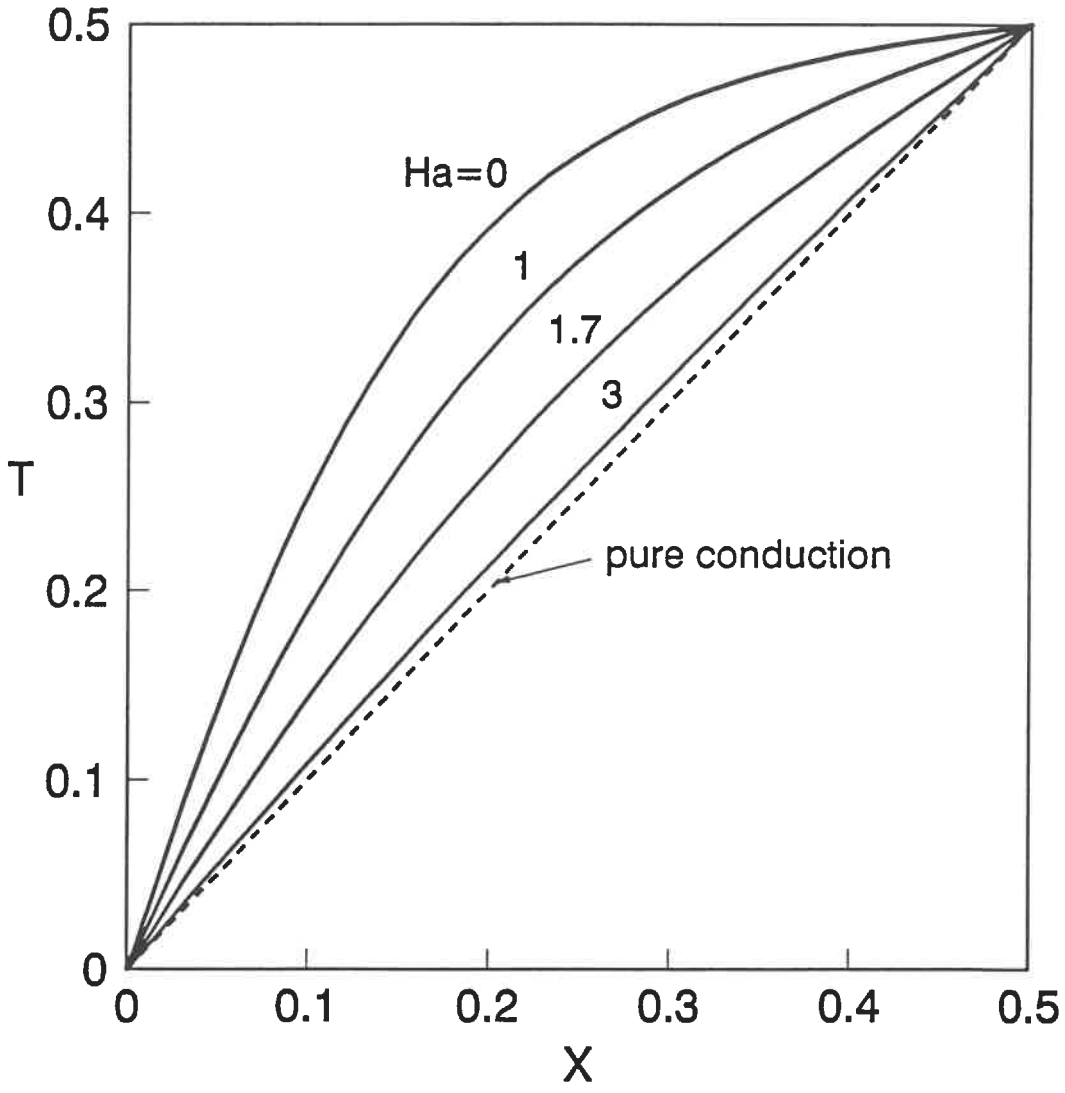

Fig. 6 The temperature profiles at mid-height of the cavity as a function

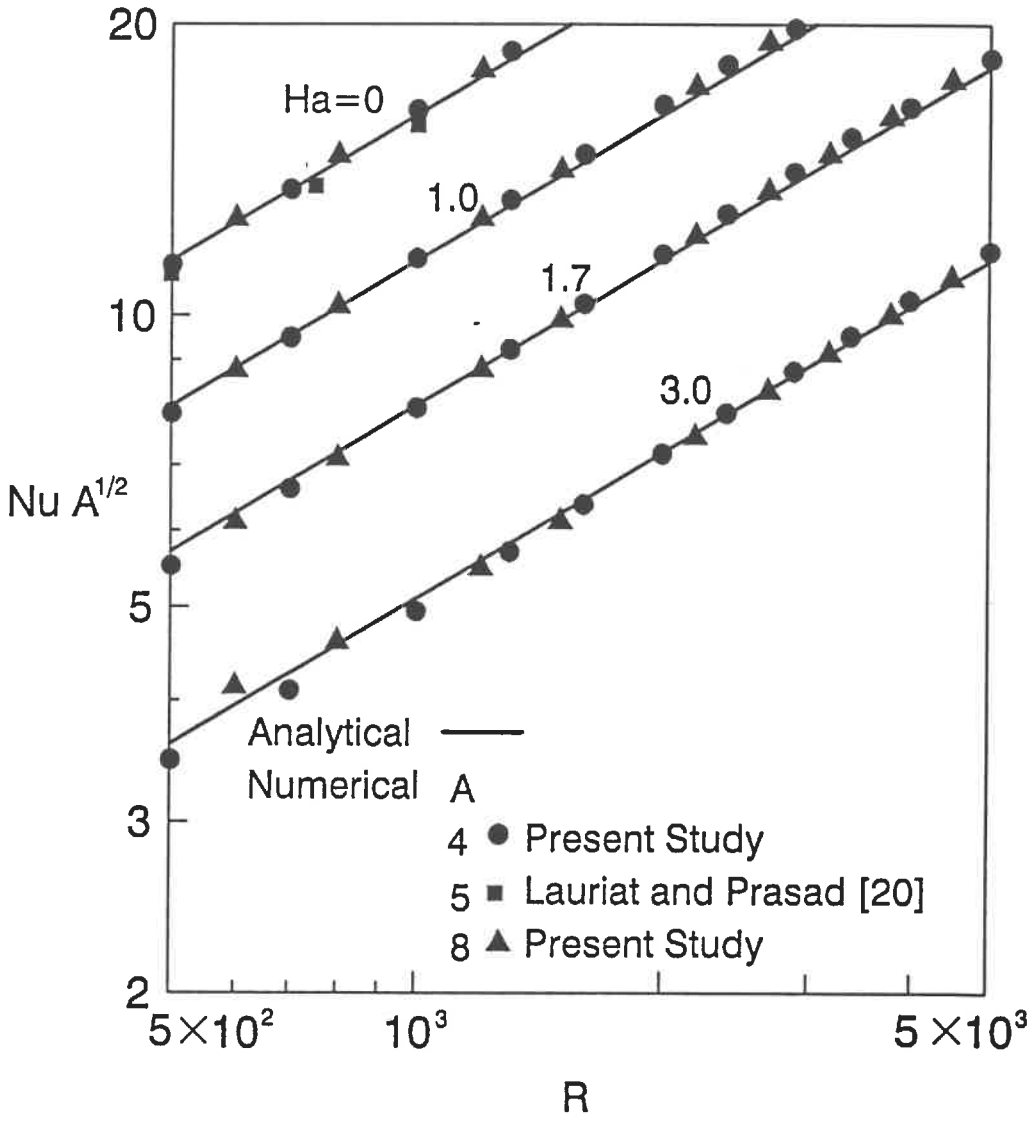

Fig. 7 Effect of the Rayleigh number on the Nusselt number for $\theta = 90^0$ and various values of the Hartmann number

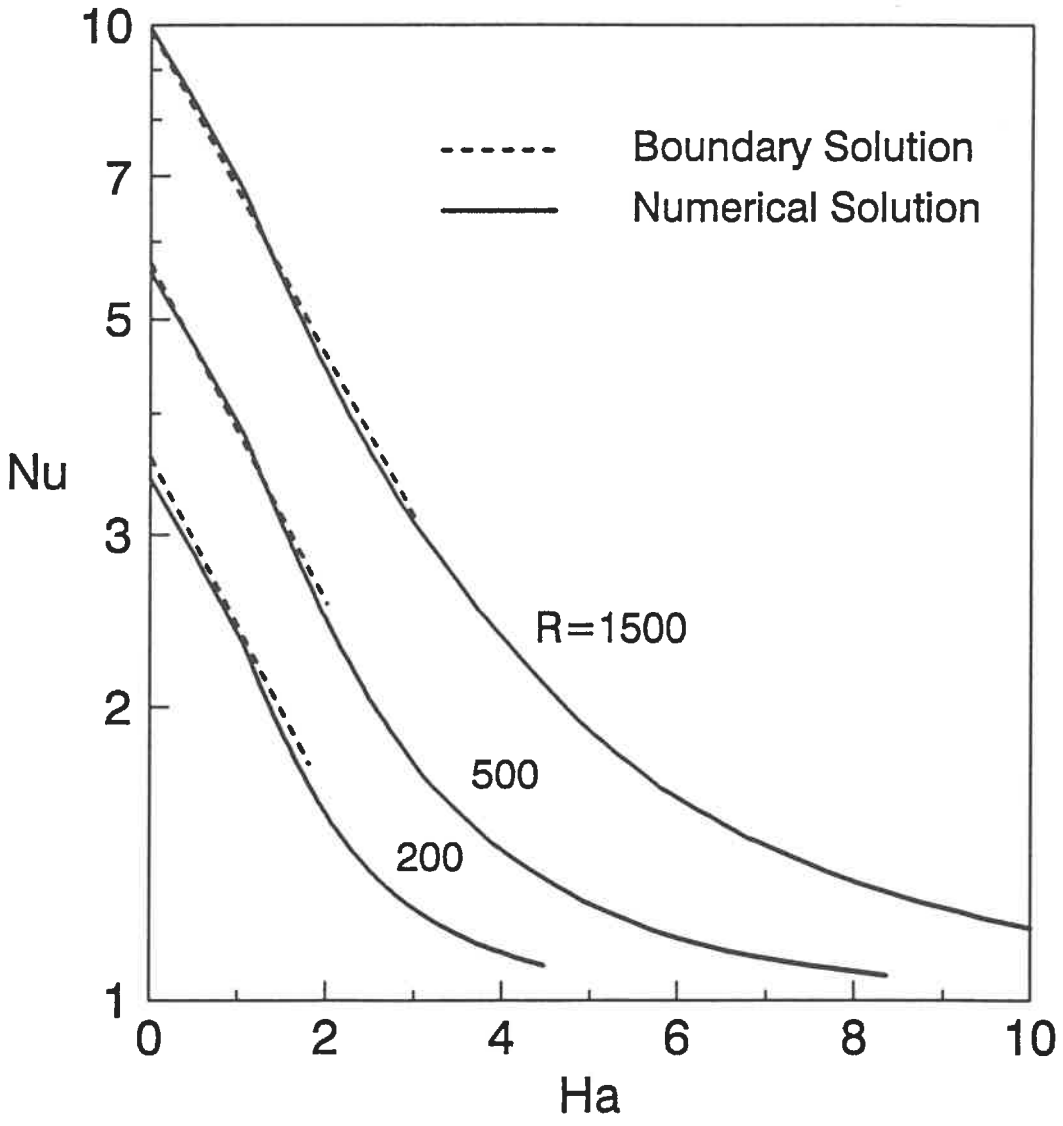

Fig. 8 Effect of the Hartmann number on the Nusselt number for $\theta = 90^0$ and various values of the Rayleigh number

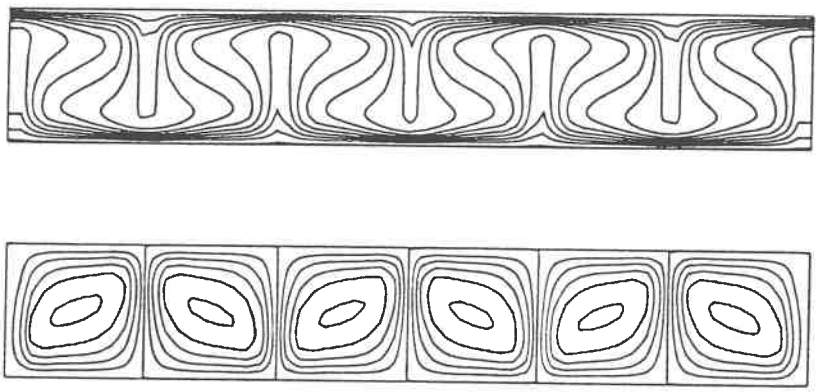

a)

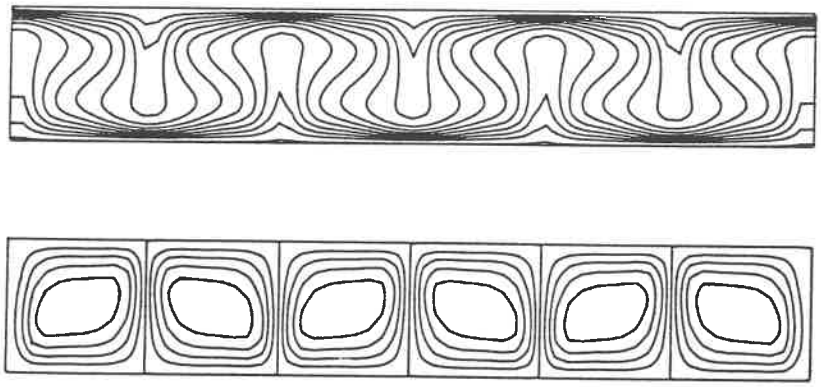

b)

Fig. 9 Computed contour maps of the streamfunction and isothermal lines for a horizontal cavity heated from below

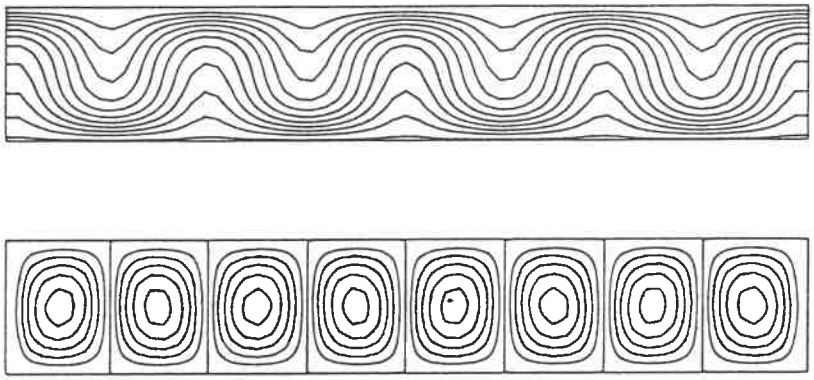

c)

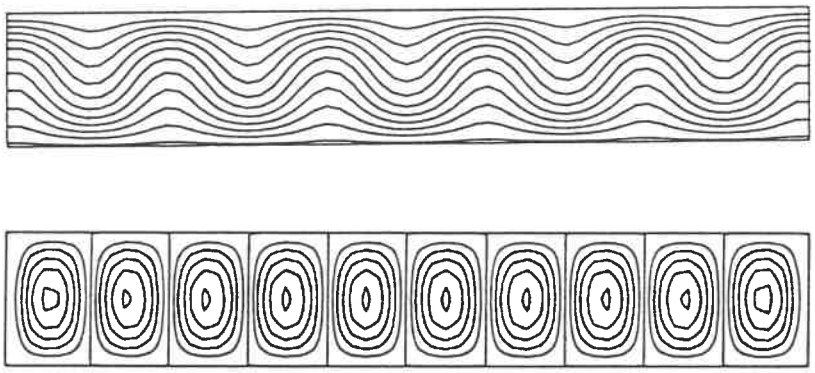

d)

Fig. 9 (Continual)

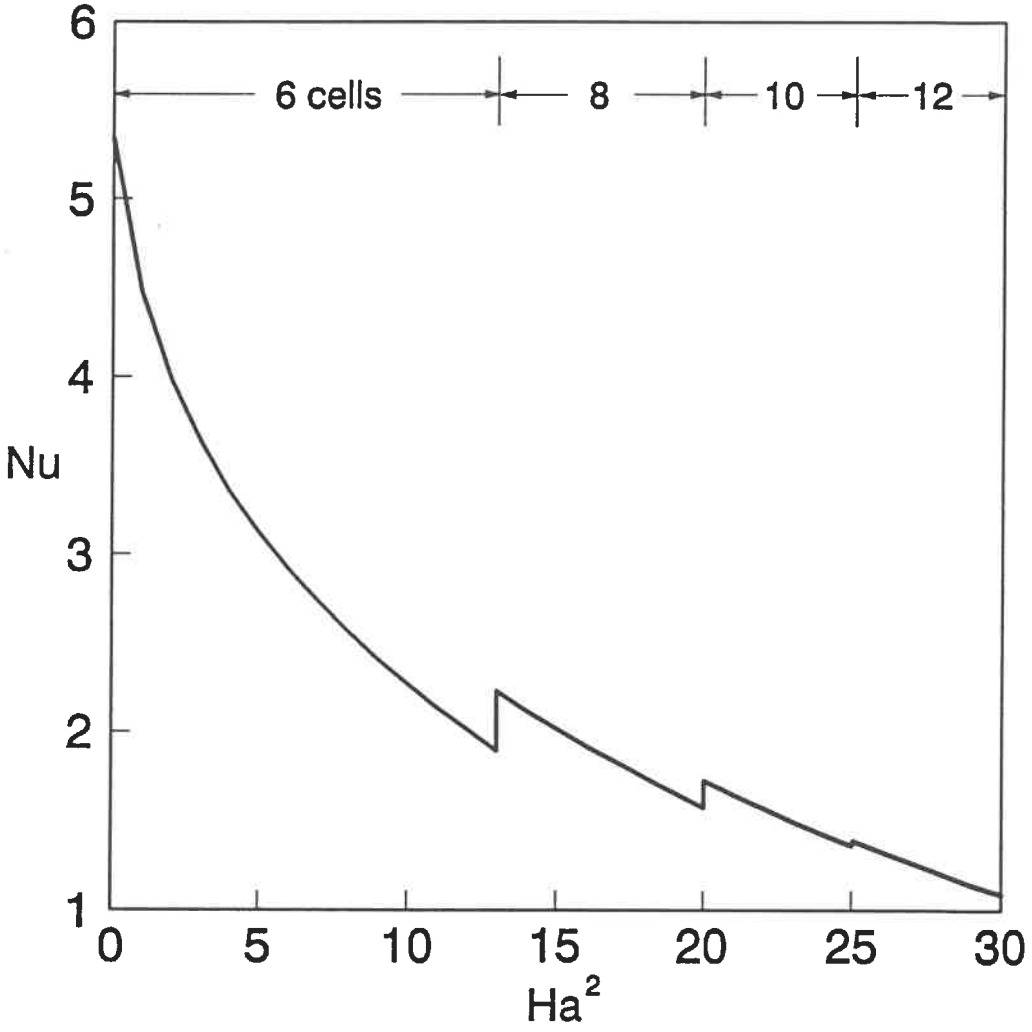

Fig. 10 Nusselt number Nu versus Hartmann number Ha

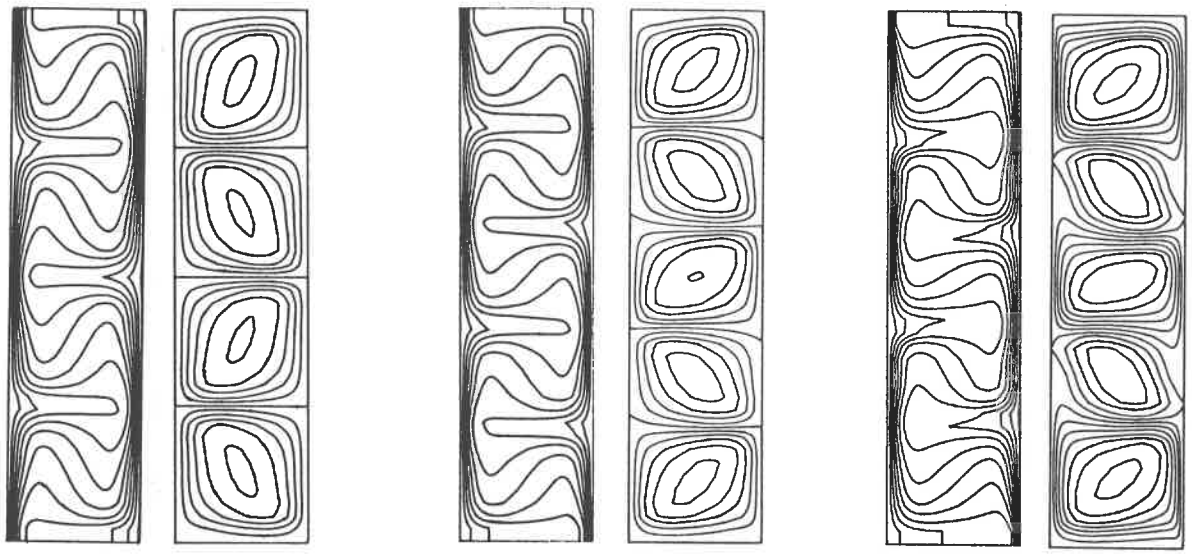

a) b) c)

Fig. 11 Computed contour maps of the streamfunction and isothermal lines for an inclined cavity

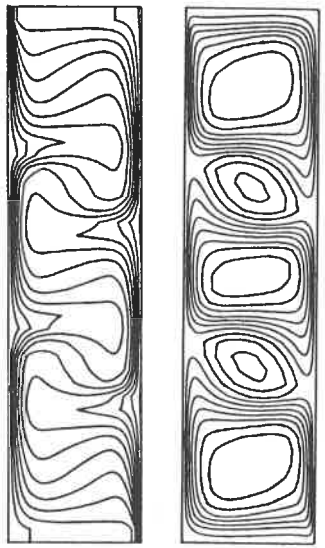

d)

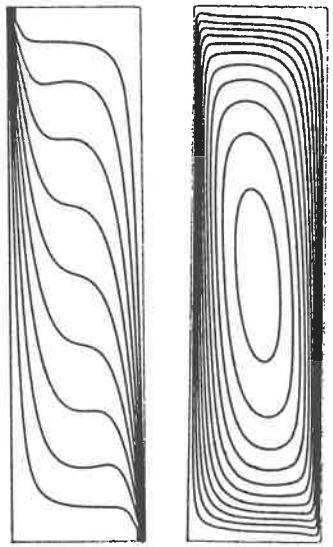

e)

Fig. 11 (Continual)

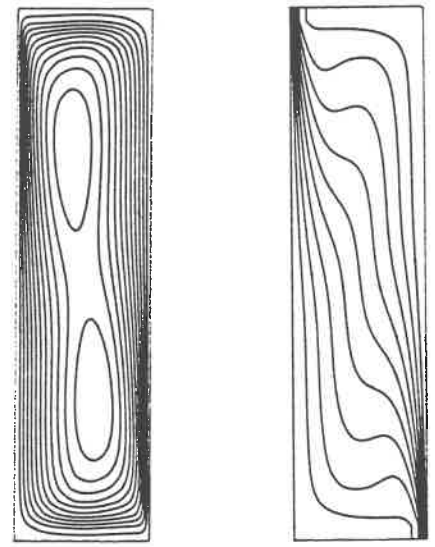

a)

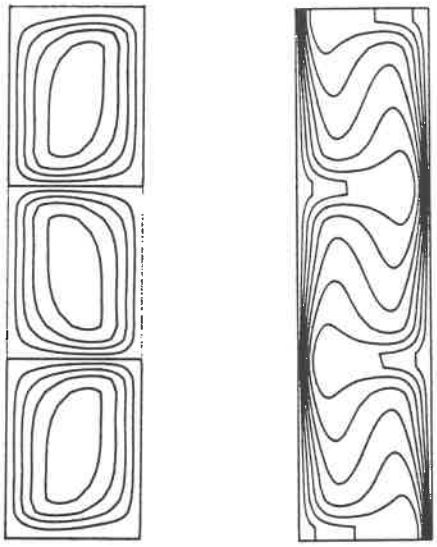

b)

Fig. 12 Computed contour maps of the streamfunction and isothermal lines for an inclined cavity

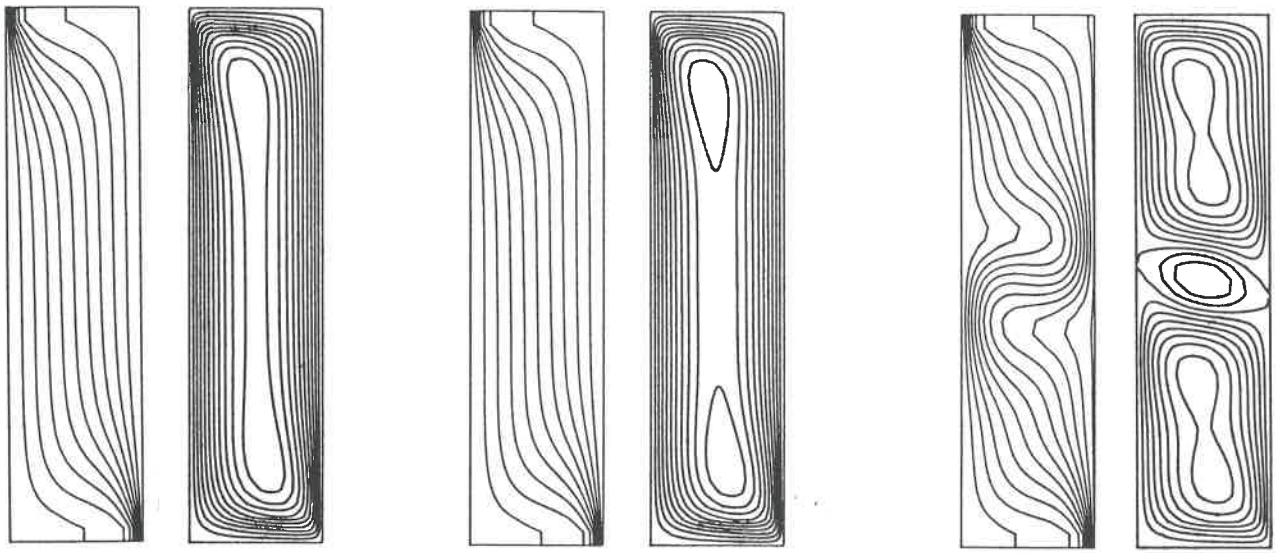

Fig. 13 Computed contour maps of the streamfunction and isothermal lines for an inclined cavity

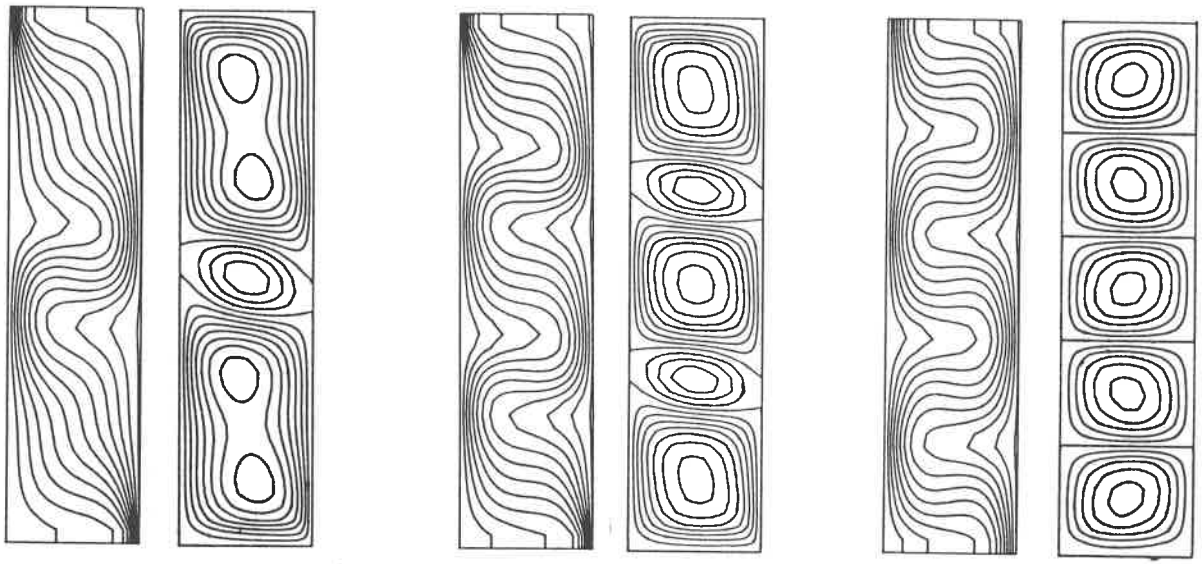

d) e) f)

Fig. 13 (Continual)

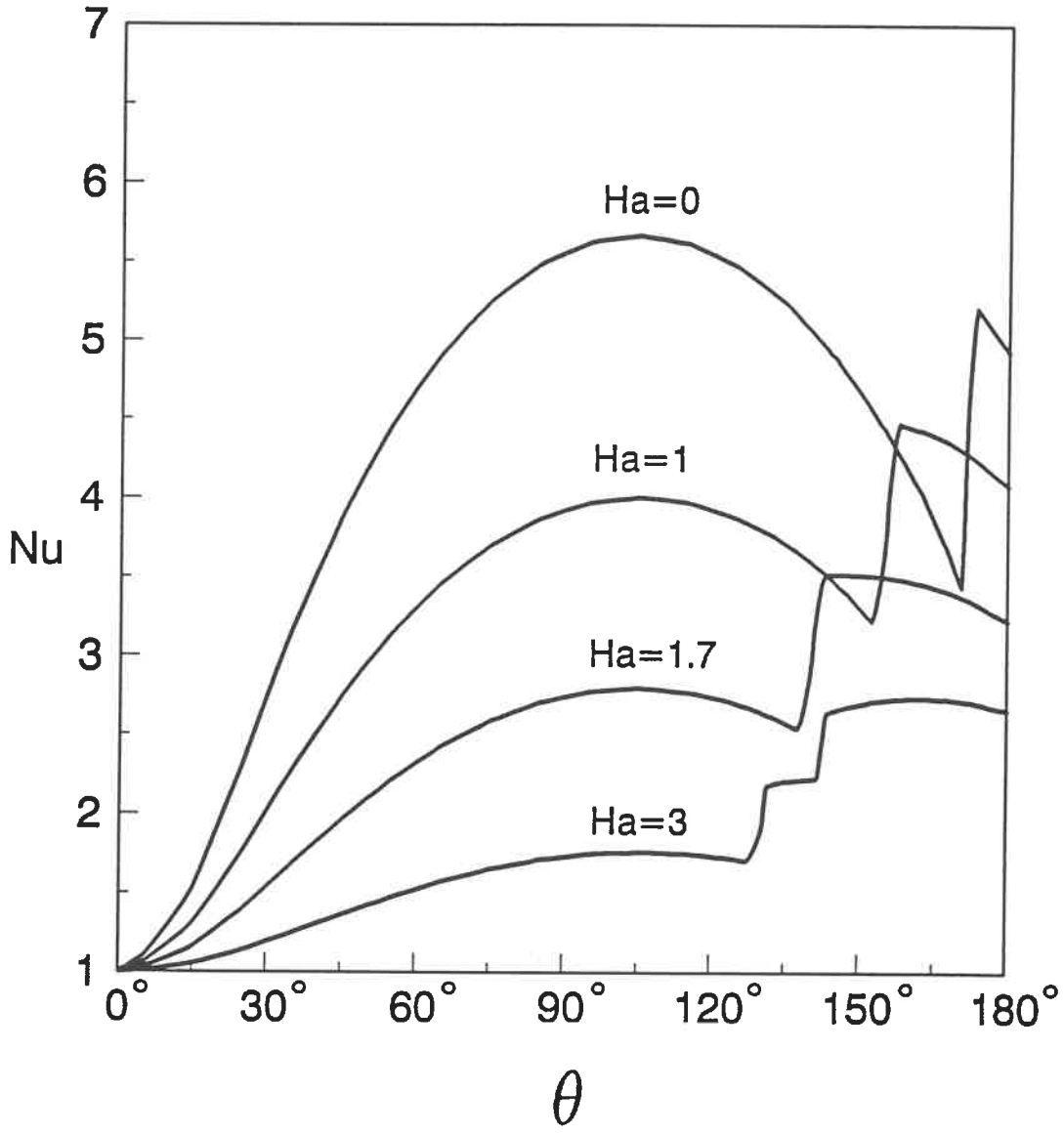

Fig. 14 Effect of inclination angle on the Nusselt number for $A = 4$, $R = 500$ and various values of the Hartmann number

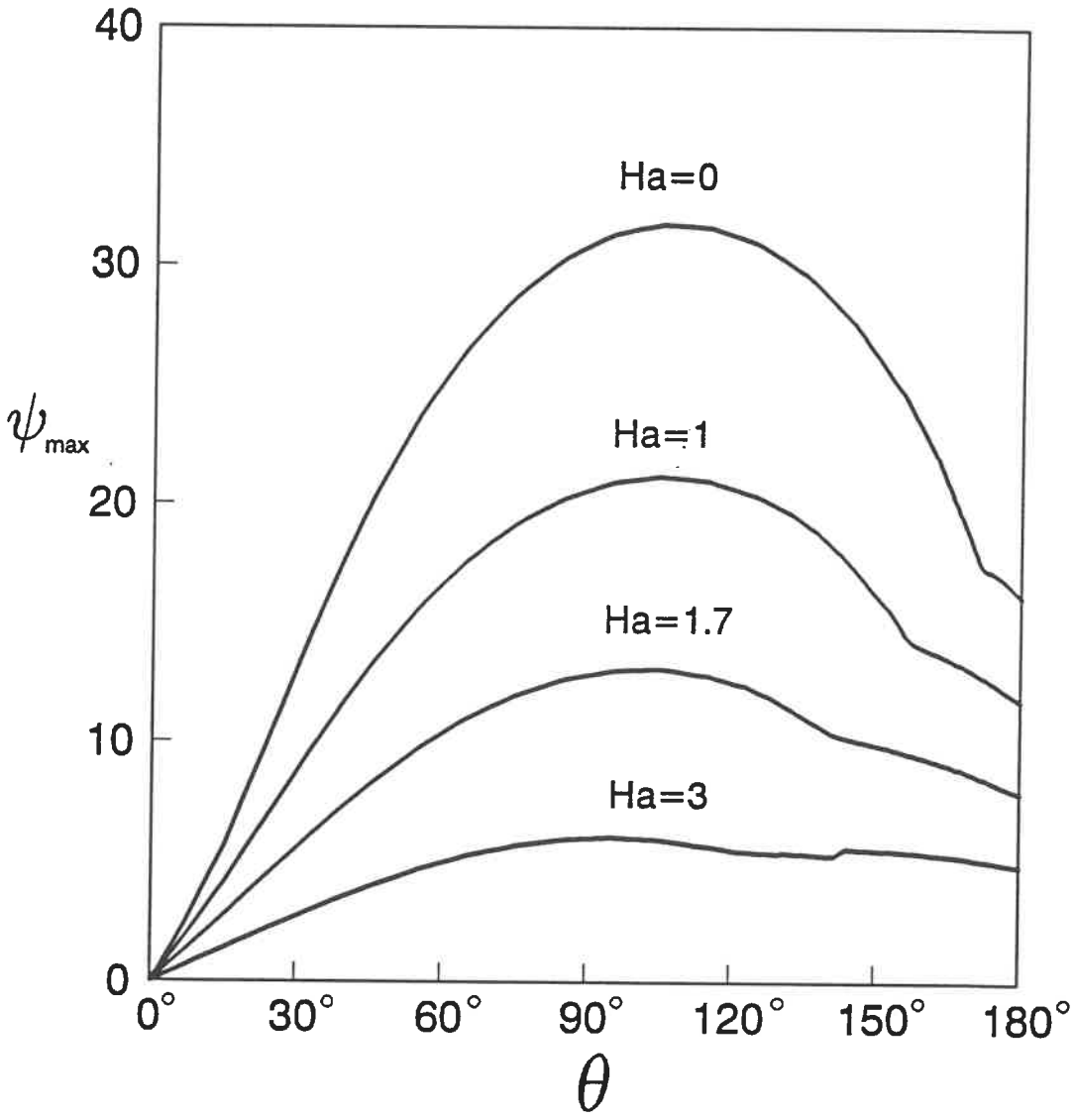

Fig. 15 Effect of inclination angle on the streamfunction for $A = 4$, $R = 500$ and various values of the Hartmann number

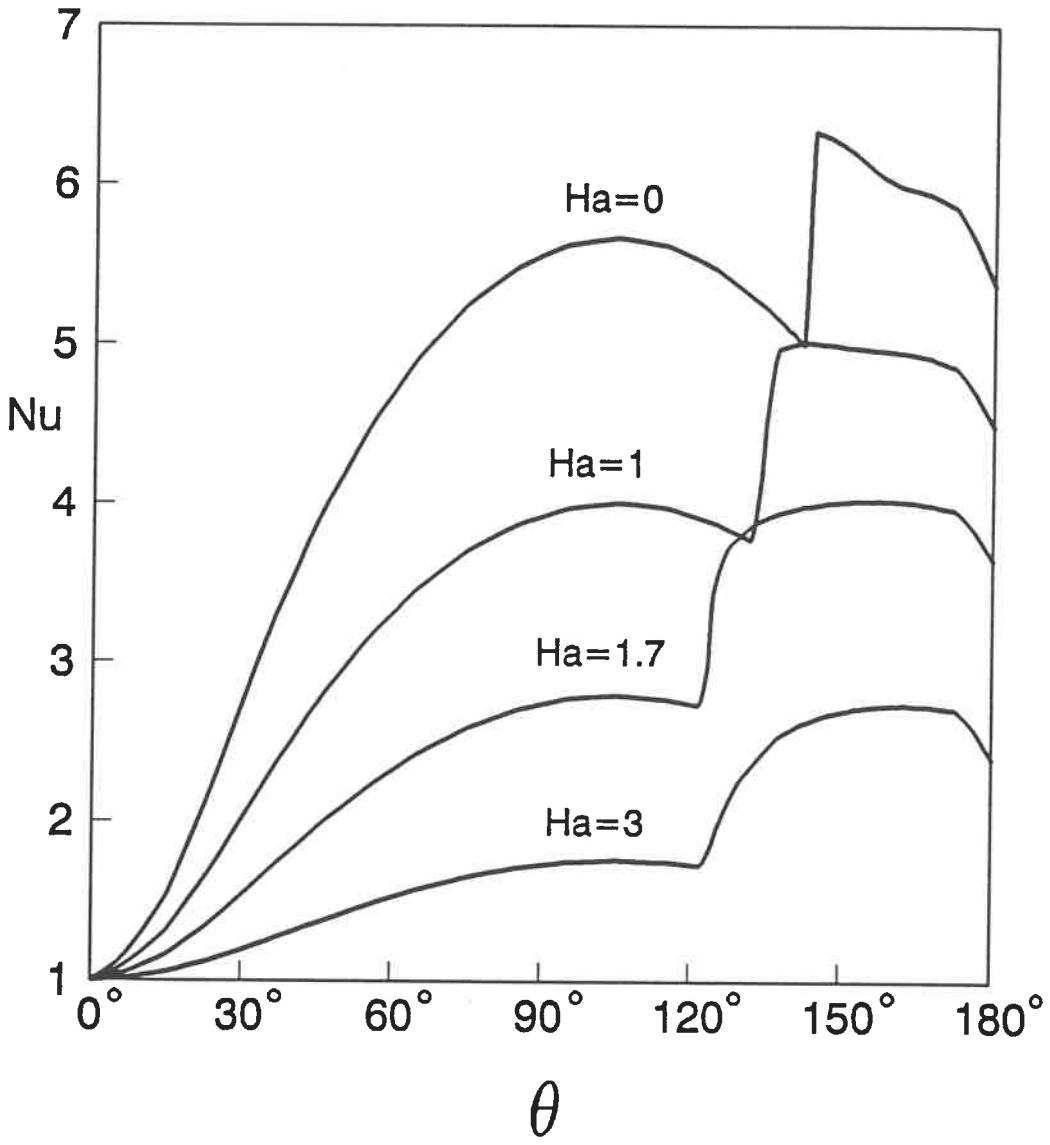

Fig. 16 Effect of inclination angle on the Nusselt number for $A = 4$, $R = 500$ and various values of the Hartmann number

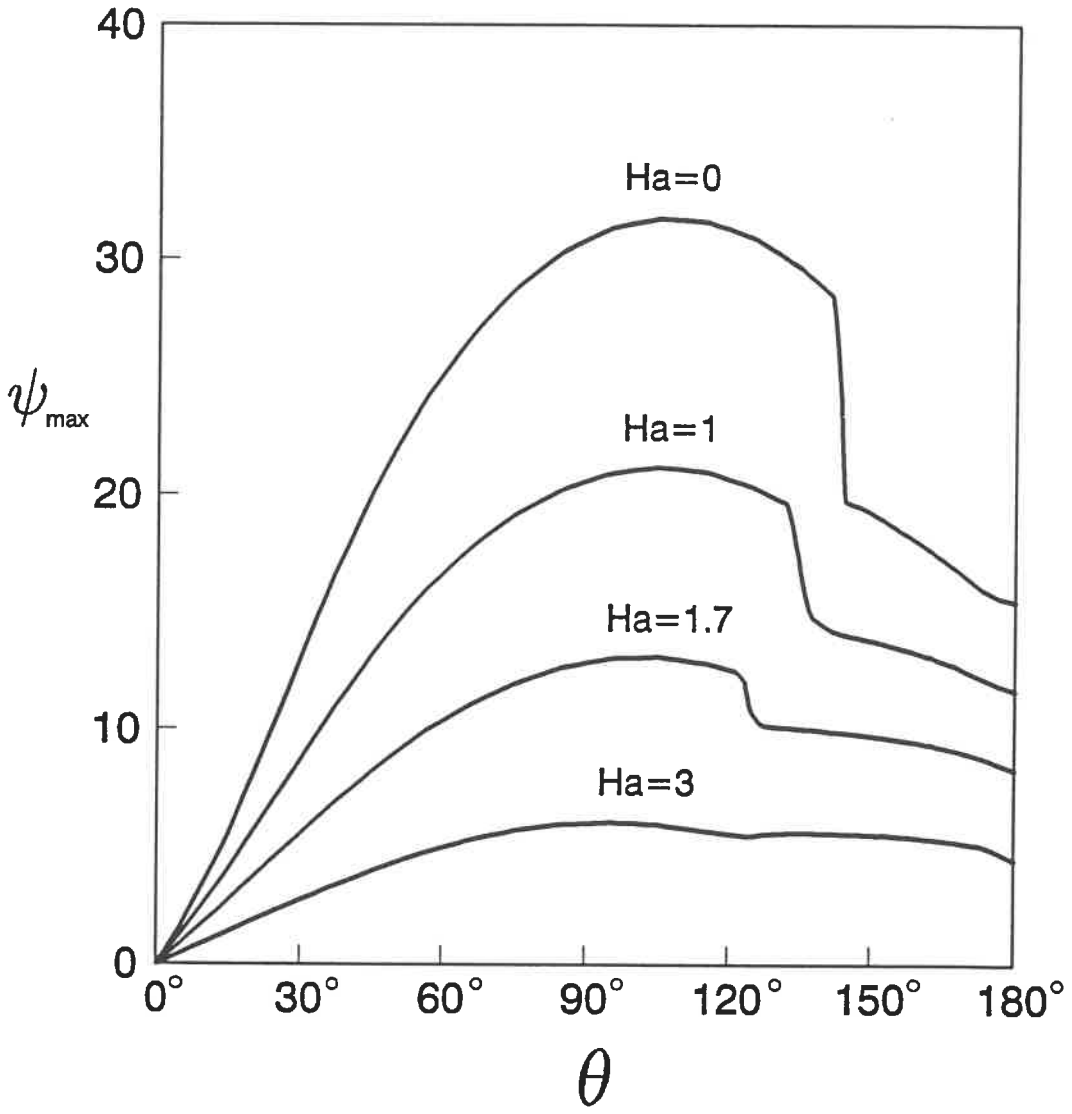

Fig. 17 Effect of inclination angle on the streamfunction for $A = 4$, $R = 500$ and various values of the Hartmann number